PNAS
www.pnas.org

Supplementary Information for

Earth history and the passerine superradiation

Oliveros, Carl H., Daniel J. Field, Daniel T. Ksepka, F. Keith Barker, Alexandre Aleixo, Michael J. Andersen, Per Alström, Brett W. Benz, Edward L. Braun, Michael J. Braun, Gustavo A. Bravo, Robb T. Brumfield, R. Terry Chesser, Santiago Claramunt, Joel Cracraft, Andrés M. Cuervo, Elizabeth P. Derryberry, Travis C. Glenn, Michael G. Harvey, Peter A. Hosner, Leo Joseph, Rebecca Kimball, Andrew L. Mack, Colin M. Miskelly, A. Townsend Peterson, Mark B. Robbins, Frederick H. Sheldon, Luís Fábio Silveira, Brian T. Smith, Noor D. White, Robert G. Moyle, Brant C. Faircloth

Corresponding authors:
Carl H. Oliveros, Email: oliveros@lsu.edu
Brant C. Faircloth, Email: brant@lsu.edu

This PDF file includes:

Supplementary text
Figs. S1 to S10
Table S1 to S3
References for SI reference citations

Other supplementary materials for this manuscript include the following:

Supplementary Files S1 to S3

www.pnas.org/cgi/doi/10.1073/pnas.1813206116

Supplementary Information Text

Extended Materials and Methods

Library preparation and sequencing. We extracted and purified DNA from fresh muscle tissue, liver tissue, or toepad clips from 113 vouchered museum specimens (Supplementary File S1) using the Qiagen DNeasy Blood and Tissue Kit following the manufacturer's protocol. We quantified DNA extracts using a Qubit fluorometer, and we prepared aliquots of DNA extracted from muscle and liver at 10 ng/μL in 60 μL volume for shearing. We sheared each DNA sample to 400–600 bp using a Qsonica Q800R sonicator for 15–45 cycles, with each cycle running for 20 seconds on and 20 seconds off at 25% amplitude. We did not shear DNA extracted from toepads. We then performed end repair, A-tailing, and adaptor ligation reactions using Kapa Biosystems Hyper Prep Kits following the manufacturer's protocol at ½ the recommended volume. We incorporated sample-specific dual-indexes to library fragments by ligating universal iTru stubs (1) to DNA during adaptor ligation and performing 8–12 cycles of PCR with iTru dual-indexed primers (1) and Kapa Hifi Hotstart ReadyMix. Following stub ligation and amplification, we purified libraries prepared from toepad clips with a higher ratio (3X) of Solid Phase Reversible Immobilization (SPRI) beads than recommended in the Hyper Prep Kit in order to retain small fragments (2).

We pooled sets of eight samples at equimolar ratios prior to enrichment, and we enriched UCE loci and performed post-enrichment amplification following standard protocols (3) using the Mycroarray MYbaits kit for Tetrapods UCE 5K version 1, which targets 5,060 UCE loci. This procedure involved hybridizing biotinylated RNA probes with pooled libraries for 24 h, capturing DNA targets using streptavidin-coated beads, and amplifying fragments with an 18-cycle PCR amplification step using Kapa Hifi Hotstart ReadyMix. After post-enrichment amplification, we measured fragment size distributions using an Agilent 2100 Bioanalyzer and removed remaining adapter-dimer using a 1.2X SPRI bead clean up. We quantified final libraries using an Illumina Eco qPCR System and a Kapa Biosystems Library Quantification Kit, combined libraries into a 10 nM pool, and sequenced the pooled libraries in a high throughput, paired-end run of 300 cycles (PE150) on an Illumina HiSeq 3000 System at the Oklahoma Medical Research Facility (OMRF). We received demultiplexed fastq data from OMRF and trimmed low-quality bases and adaptor sequences from reads using illumiprocessor ver. 2 (https://github.com/faircloth-lab/illumiprocessor).

Data assembly. After trimming the demultiplexed sequence data, we assembled them using two approaches implemented in the open-source Python package PHYLUCE (4). For tissue-derived sequence data, we assembled reads into contigs using Trinity ver. trinityrnaseq-r2013-02-25 (5), and for toepad-derived data, we assembled reads into contigs using Spades ver. 3.9.0 (6). We then grouped these new assemblies with the assemblies from previous work and the *in silico* data collected from genomes (Supplementary File S1), and we performed the remaining data preparation steps using PHYLUCE (4) following a standard protocol (7). Specifically, we used PHYLUCE to identify those contigs that were enriched UCE loci, collect summary statistics from assembled loci, align assembled loci using MAFFT (8), trim the edges of aligned loci to ensure each edge retained data for at least 65% of taxa, and internally trim the aligned loci using Gblocks (9) with the minimum number of sequences for a flank position (-b2) changed from the default value to 65%. After trimming alignments, we assembled a data set containing UCE loci that were present in at least 80% of all 221 taxa.

Topology estimation. We used both concatenation and coalescent approaches to estimate phylogenetic relationships among passerines. We performed maximum likelihood (ML) inference on the concatenated dataset using ExaML ver. 3.0.15 (10) assuming a general time reversible model of rate substitution and gamma-distributed rates among sites. We evaluated node support using 100 bootstrap replicates, and we tested for convergence of bootstrap replicates *a posteriori* using the 'autoMRE' option in RAxML 8.2.8 (11). We also used four coalescent approaches to species tree estimation: (a) SVDquartets (12, 13), which uses singular value decomposition of the matrix of site pattern frequencies of quartets from SNP or genome-scale sequence data to build a species tree and does not rely on prior estimation of gene trees; (b) ASTRID

(14), a more efficient implementation of NJ-st (15), a method that estimates the species tree from a matrix of average node distances between tips in gene trees; (c) ASTRAL-II (16), which searches for a species tree that maximizes the number of component quartets in gene trees that are compatible with the species tree; and (d) STEAC (17), which estimates the species tree from a matrix of average coalescence times from estimated gene trees. Although not strictly a coalescent method, ASTRAL II is statistically consistent under the multi-species coalescent model. We estimated gene trees using RaxML ver. 8.2.8 (11), and we analyzed gene trees with ASTRID ver. 1.3 (14), ASTRAL II ver. 4.10.11 (16), and STEAC as implemented in the R package phybase ver. 1.4 (17). We evaluated nodal support for ASTRID, ASTRAL, and STEAC by generating 100 multilocus bootstrap replicates (18) using PHYLUCE (4). We performed SVDquartets (12, 13) analysis by generating all quartet trees by singular value decomposition in PAUP* ver. 4.0a150 (19), and we assembled species trees from quartets using the quartet max-cut method as implemented in the program max-cut-tree ver. 3.0 (20). We estimated nodal support by performing SVDquartets analyses on the same 100 bootstrap replicates we generated for ML analysis.

Concatenation and coalescent analyses can estimate species trees that are highly supported but conflict with one another within and across paradigms (21, 22). Some of these differences can be attributed to biased gene-tree estimation caused by missing data (23–26). We observed these conflicts among methods for the placement of 27 taxa (Figs. S1–S5). To address this issue, we performed ASTRID, ASTRAL, and STEAC analyses of 15 subsets of the data matrix (Table S3, Supplemental File S2) each with 10–40 taxa and with individual locus alignments trimmed to the length of one or two target taxa to minimize missing data in the flanks of each alignment (23). These additional analyses eliminated most of the highly supported inconsistencies across methods; only five taxa had highly supported conflicting placements following these analyses (Fig. S1; Supplementary File S2). For these remaining inconsistencies, we adopted the ML topology, unless coalescent approaches provided a consistent contradicting topology, which was observed only in the placement of *Peltops* and *Calyptophilus* (Figs. S2–S5). We used this 'reconciled' topology for subsequent divergence time, biogeographic, and diversification analyses.

Divergence time estimation

Fossil calibrations. The passerine fossil record is rich, but the vast majority of passerine fossils are either too young to be useful for dating deep phylogenetic divergences or too fragmentary to be confidently placed in a family-level phylogeny (27). The fossilized birth-death model provides a way of dating phylogenies using fossils with uncertain phylogenetic position (28). However, this model assumes a constant speciation and extinction rate and a uniform fossil recovery rate throughout the tree: assumptions that are unrealistic for the large and sometimes rapid radiation of passerines. To avoid violating these assumptions, we followed a more traditional divergence time estimation approach in which we used best practices for justifying fossil calibrations (29) to select and assign nine passerine and four non-passerine fossils to specific nodes (see **Fossil Calibrations** section below). To examine the sensitivity of our date estimates to the inclusion or exclusion of particular calibration points, we performed analyses with three sets of fossil calibrations: Set A, which included all 13 fossils; Set B, which included a calibration at the root of the phylogeny, one at the split of passerines with parrots, and five others at key passerine nodes; and Set C, which included a single calibration at the root (Fig. 3). We also investigated the effects of prior distribution choice on our date estimates by performing dating analyses using two prior settings for each set of calibration points: the first used an uninformative, uniform prior on each calibration point and the second applied a lognormal distribution with *log*(mean)=0 and *log*(standard deviation)=1 and the same minimum and maximum values as the uniform prior on each calibration point. We did not use empirically derived prior distributions on our fossil calibrations (30) because of low sample sizes for generating distributions at some nodes. Date estimates based on uniformly distributed priors were 1–6 Ma older than dates obtained using lognormally distributed priors, with the disparity greater for deeper nodes. We used dating results from analyses of lognormally distributed priors in subsequent biogeographic and diversification analyses because, based on theoretical and empirical considerations, the uncertainty regarding clade age is represented better by a continuously decreasing probability function, rather than discrete upper bounds (30, 31). To examine the sensitivity of age estimates at deeper nodes to the use of much older priors and possible

interactions among calibrations, we also performed analyses using an excessively old maximum age with the lognormal prior for both fossil calibration Sets A and C. Specifically, we used an upper limit of 80 Ma for nodes for which we had originally set the upper limits to 66.5 Ma or 56.0 Ma. This upper limit exceeds the age of the oldest known crown bird fossil and, as a result, represents an extremely loose upper bound.

Approach. Performing divergence time analysis with large data sets is challenging because of computational limitations. For example, using more data can help inform estimation of branch lengths and, therefore, node ages, but software packages that can analyze large data sets generally implement simpler models of sequence evolution. Conversely, software that implements more complex models of sequence evolution can only reliably analyze relatively small datasets, and dating approaches based on the multispecies coalescent are computationally intractable for many tips or many loci. To address these discrepancies, we took two analytical approaches to divergence time estimation: (a) we analyzed small subsamples of loci using BEAST and a more complex model of sequence evolution, and (b) we analyzed the concatenated dataset using MCMCTree and a simpler model of sequence evolution. For both approaches, we fixed the tree topology to the reconciled topology between ML and coalescent analyses that we described above. We compared divergence time estimates among the two approaches by comparing them to each other, and to other studies (25, 30, 32, 33), using R ver. 3.3.2 and the R package ggplot2 ver. 2.2.1.

Dating with BEAST. We drew 10 random samples of 25 UCE loci from our dataset using a custom Python script so that each locus had at least 95% of taxa sampled. For each random sample and for each set of fossil calibrations, we executed 8 independent MCMC runs using BEAST ver. 1.8.4 (34) with different starting seed numbers. For each MCMC run, we assumed a generalized time reversible model of sequence evolution with gamma-distributed rates in four categories, an uncorrelated relaxed clock model with lognormal distribution on the rate prior, and a birth-death model with incomplete sampling on the tree prior. We ran each chain for 14–19 million generations sampling every 5000 generations, and we checked each run for convergence of parameter values and age estimates by inspecting traces and effective sample sizes in Tracer ver. 1.6.0 (35). We then combined tree and log files from each set of 8 independent runs using TreeAnnotator ver. 1.8.4 (36) and LogCombiner ver. 1.8.4 (37) removing 2 million generations as burnin and resampling every 20 thousand generations. We then re-checked the combined log files for convergence using Tracer under the criteria previously described. To assess the level of rate heterogeneity across the tree, we examined the coefficient of variation in clock rates among lineages from the combined BEAST log files. We also generated joint prior distributions for each set of fossil calibrations by running MCMCs with no data (38). Finally, to assess the effects of among-lineage rate variation on our date estimates, we analyzed one subsample of the 25 most clock-like loci that we identified using SortaDate (39). Specifically, we sorted loci by root-to-tip variance, then by bipartition support, and finally by tree length, selected the 25 most clock-like loci, and input these loci to a BEAST analysis that used lognormal priors on calibrated nodes and followed the same procedures described above.

Dating with MCMCTree. We estimated divergence times in MCMCTree (40); PAML ver. 4.8 package) with the concatenated data matrix treated as a single locus. We assumed a model of independent rates among branches drawn from a lognormal distribution with gamma-distributed hyper-priors for the mean and variance of rates and a birth-death-sampling model of lineage diversification. We applied the HKY85 + GAMMA model of nucleotide substitution with four rate categories, a simpler model compared to what was used in BEAST analyses but the most complex model implemented in MCMCTree. Because of the size of the data matrix, we used approximate likelihood calculations with branch lengths estimated using the baseml program of PAML. We ran four independent MCMC chains with parameters sampled 5×10^4 times every 2×10^3 generations after discarding 2×10^5 generations as burn-in. We assessed convergence of likelihood and parameters by examining trace plots in Tracer ver. 1.6 (35) and by comparing results between independent runs. We also ran MCMCs with no data to generate joint prior distributions (38).

Biogeographic analysis

The goal of the biogeographic analyses was to examine broad patterns of avian dispersal across the following major land-masses: North and Central America and the Caribbean (A, referred to as North/Central America); South America (B); Africa and Madagascar (C, referred to as Africa); the Palearctic and Indomalaya east to Wallace's line (D, referred to as Eurasia); and Wallacea, Australia, New Guinea, New Zealand, and the Pacific (E, referred to as the Australo-Pacific). We coded each tip by the total geographic distribution of members of the clade the tip represents based on published phylogenies, and we ignored distributions of clade members that marginally occured in an area. This approach of using the total geographic distribution for higher taxa was the best option for our data to avoid potential biases introduced when using non-randomly sampled species (which we have done here) or polytomy resolvers (41). Furthermore, we did not use the inferred origin of clades represented by the tips because this would have required knowledge of the crown age of each clade for insertion into the tree. Using the R package BioGeoBEARS ver. 0.2.1 (42) in R ver. 3.3.2 (43), we compared ancestral area estimates using likelihood versions of the dispersal-extinction-cladogenesis (DEC) model (44, 45) and the DEC + *j* model (46) under two scenarios: one that allowed dispersal between all areas and another that limited dispersal to movement between adjacent areas. Under the first scenario, we used a matrix of dispersal multipliers with a value of 1.0 between all pairs of areas. For the second scenario, we used a dispersal multiplier value of 0.01 between non-adjacent areas and a dispersal multiplier value of 1.0 between all other areas. Under this second scenario, we considered the following area pairs non-adjacent: A and C, A and E, B and C, B and D, B and E, and C and E. The models that restricted dispersals between non-adjacent areas produced significantly higher likelihood values compared to their counterparts with unrestricted movement between areas (Table S3), so we present only reconstructions based on the restricted dispersal models. The DEC + *j* model has recently been criticized for parameterizing the mode of speciation and not being statistically comparable to the DEC model (47). Here, we do not perform statistical model selection between DEC and DEC + *j* models but present both results, because we believe the debate regarding the validity of the DEC + *j* model is an open issue and also that jump-dispersal speciation is a reasonable model for passerines.

To examine the effects of including closely related fossil taxa on ancestral area estimates of major passerine lineages, we performed a series of biogeographic analyses that included the following four fossil taxa: (a) Halcyornithidae: North American and European distribution, age 53.5 Ma, sister to Passeriformes + Psittaciformes; (b) Zygodactylidae: North American and European distribution, age 51.8 Ma, sister to Passeriformes; (c) *Wieslochia*: European distribution, age 31.5 Ma, either sister to suboscines or sister to suboscines + oscines; and (d) Australian QM F20688: Australian distribution, age 54.6, either sister to Zygodactylidae + Passeriformes, sister to Zygodactylidae, or sister to Passeriformes. Using an R script adapted from (30), we inserted fossil taxa at the midpoint of the stem branch of their sister clade. Because of the uncertain phylogenetic positions of *Wieslochia* and Australian QM F20688, we performed biogeographic analysis on a total of six topologies that reflect the different combinations of placements for these taxa.

Diversification rate analysis

*Episodic diversification rate***.** Because we were interested in understanding whether passerine diversification was correlated with Cenozoic global temperature (48), we examined passerine diversification rates using models that assume a birth-death process in which speciation and extinction rates vary episodically through time by piecewise constant rates (49, 50) as implemented in RevBayes ver. 1.0.3 (51). To account for missing taxa, we used an empirical taxon sampling strategy (52) by assigning the number of missing species for each clade based on taxonomy (53) and published phylogenies. We employed a reverse-jump MCMC analysis between a model in which changes in the logarithm of speciation (and extinction) rates were proportional to changes in global temperature (52), and a model that did not include global temperature as a factor. We ran four independent MCMC chains of 2×10^5 generations, after a burn-in run of 1×10^5 generations, with a tuning interval of 200. We assessed convergence by examining trace plots in Tracer ver. 1.6 (35) and by comparing results between independent runs. Logs from the independent

runs were combined using LogCombiner ver. 1.8.4 (37). We assessed relative model support using Bayes Factors, which we calculated by dividing the posterior odds ratio by the prior odds ratio (52). We plotted estimated episodic diversification rates using the R package RevGadgets (51).

Lineage-specific diversification rates. To examine diversification rate shift configurations within passerines, we estimated lineage-specific diversification rates using BAMM (54). To prepare the data for input into BAMM, we used the reconciled dated tree as a baseline for diversification analyses, allowing lineage-specific speciation and extinction. We assigned diversities to each sampled tip based on taxonomy (53) and previously published phylogenetic analyses of passerine clades, where necessary. Using code in R ver. 3.3.2 (43), we replaced each tip in the original tree representing more than one species with a randomly-generated phylogeny having the appropriate number of tips using the *rphylo*() function of *ape* ver. 5.0, using a lineage-specific pure-birth estimate of the diversification rate based on the number of tips in the clade and the stem age. We rejected subclade trees until their crown age was less than the target clade's stem age, then we grafted each onto the original tree to replace the original tip. We repeated the grafting process to generate 100 random-grafting replicates with diversities matching the number of extant passerines (6,054 species).

We analyzed lineage-specific diversification rates for replicate trees using *BAMM* (54), setting priors using the *setBAMMpriors*() function of BAMMtools ver. 2.5.0, the expected number of rate shifts to 1, and analyzing each replicate for 2×10^6 generations, sampling every 1000, using four Metropolis-coupled Markov chains with a heating parameter of 0.1 and default scaling operators and move frequencies. Subsequently, we imported event data into R using *getEventData*() with a 50% burn-in, and we summarized these data using code that filtered results to remove events occurring within grafted subclades, retaining only events that occurred on the original backbone tree or at the base of grafted clades. To assess where shifts were best supported, we estimated branch-specific marginal odds ratios for each replicate using the BAMM function *marginalOddsRatioBranches*(), eliminated branches not found on the original tree, and then calculated the median ratio for each remaining branch across replicates (Fig. S10).

Fossil Calibrations

Calibration 1: Root (basal split in Australaves)

Minimum Age: 53.5 Ma

Maximum Age: 66.5 Ma

Fossil Taxon: *Pulchrapollia gracilis*

Specimen: NHMUK A6207, partial skeleton

Reference: (55)

Phylogenetic Justification: *Pulchrapollia gracilis* is a member of the extinct clade Halcyornithidae (=Pseudasturidae). This group was initially considered to represent stem lineage Psittaciformes (55–57). However, more recent phylogenetic analyses (58) identify Halcyornithidae as stem Psittacopasserae (i.e., sister taxon to Psittaciformes and Passeriformes). We concur with these results, and given that no other well-constrained older records of Australaves fossils are known, *Pulchrapollia gracilis* provides a minimum age for the root of our tree.

Locality: Walton Member (Division A2) of the London Clay Formation at Walton-on-the-Naze, England.

Age Justification: The Walton Member correlates to the upper part of Chron C24r, and the minimum age is based on the youngest estimate for the top of C24r (53.54+/-0.04; 59). The oldest member of the other side of the basal split in Australaves, Cariamiformes, is *Paleopsilopterus* from Itaboraí, Brazil. The Itaboraí fossil deposits were originally considered to be Paleocene in age but have recently been re-dated to the Eocene (~53 Ma; 60) making them very close in age to the London Clay Formation. The latest Cretaceous is set as the maximum, corresponding to the age range of the oldest confirmed crown bird fossil *Vegavis*. No members of the Psittacopasserae or the more inclusive clade Telluraves ("higher land birds") are known from Cretaceous deposits, indicating it is extremely unlikely that the highly nested parrot-songbird divergence occurred before the Paleocene.

Calibration 2: Psittacopasserae (split between Psittaciformes and Passeriformes)

Minimum Age: 51.81 Ma

Maximum Age: 66.5 Ma

Fossil Taxon: *Eozygodactylus americanus*

Specimen: USNM 299821, partial articulated skeleton

Reference: (61)

Phylogenetic Justification: Phylogenetic analyses have consistently recovered Zygodactylidae (including *Eozygodactylus*) as stem passerines (e.g. 58, 62), a placement supported by a suite of characters including the presence of a large processus intermetacarpalis of the carpometacarpus, great elongation of the tarsometatarsus (exceeding length of humerus), and presence of a crista plantaris lateralis of the tarsometatarsus (58). This phylogenetic placement has been recovered by analyses of morphological data alone, and analyses in which constraint topologies for extant taxa based on various molecular phylogenies are enforced (58, 62). We selected *Eozygodactylus* over slightly older but very fragmentary remains from Australia (63) due to the much more complete nature of the material and the fact that this taxon has been included in multiple phylogenies.

Locality: Fossil Butte Member, Green River Formation, Wyoming, USA

Age Justification: We based the minimum age on the lower bound of the age for the fossiliferous horizons of the Fossil Butte Member. These deposits are late early Eocene, and multicrystal analyses (sanidine) from a K-feldspar tuff (FQ-1) at the top of the middle unit of the Fossil Butte Member have yielded an age of 51.97 ± 0.16 Ma (64). Slightly older potential records of Zygodactylidae from the London Clay Formation and Fur Formation have been referenced (65), but because the former are isolated bones and the latter are not yet formally described, we based our calibration of the hard minimum age on the more complete and well-documented Green River Formation specimens. We set the latest Cretaceous as the maximum, corresponding to the age range of the oldest well supported crown bird fossil *Vegavis.* No members of the Psittacopasserae or the more inclusive clade Telluraves ("higher land birds") are known from Cretaceous deposits, indicating it is extremely unlikely that the highly nested parrot-songbird divergence occurred before the Paleocene.

Calibration 3: Stem *Falco* **(**split between *Falco* and *Microhierax)*

Minimum Age: 16.0 Ma

Maximum Age: 48.0 Ma

Fossil Taxon: *Pediohierax ramenta* (= *Falco ramenta*)

Specimen: USNM 13898, tarsometatarsus

Reference: (66)

Phylogenetic Justification: Phylogenetic analysis by Li et al. (67) supports placement of *Pediohierax ramenta* as a crown member of Falconidae, more closely related to *Falco* than to *Microhierax* or *Polihierax*. All remains of this taxon are isolated bones, and the apomorphies supporting placement as sister taxon to *Falco* occur in the humerus and tarsometatarsus. Therefore, we selected a tarsometatarsus as the calibrating specimen.

Locality: Merychippus Quarry, Sand Canyon Member of the Sheep Creek Formation, Nebraska, USA.

Age Justification: The Sheep Creek Formation is assigned to the Hemingfordian North American Land Mammal Age (68). Thus, we used the end of the Hemingfordian as a minimum age for the calibration. There are many "raptorial" birds of uncertain affinities in the fossil record that potentially represent Falconiformes, Accipitriformes, or some separate clade. The maximum extends back to the Eocene to include the oldest such well-represented taxon, *Masillaraptor parvunguis.* This species shares some derived traits with Falconiformes, but these traits are also seen in other, distantly related raptorial clades (69). Thus, the maximum estimate conservatively encompasses all potential members of Falconidae, even though the possibility that any of these fossils represent crown falconids is remote.

Calibration 4: Crown Nestoridae (split between *Strigops* and *Nestor*)

Minimum Age: 15.9 Ma

Maximum Age: 66.5 Ma

Fossil Taxon: *Nelepsittacus minimus*

Specimen: NMNZ S.52404, tarsometatarsus

Reference: (70)

Phylogenetic Justification: Worthy et al. (70) reported several apomorphies that support a placement for *Nelepsittacus* closer to *Nestor* than to *Strigops*. The species is known from multiple isolated elements. A unique apomorphy (foramen vasculare distale bound on dorsal facies by proximally extending ridge, creating a shallow groove extending proximal of the foramen) is present in the tarsometatarsus. Thus, we selected this element as the calibrating specimen.

Locality: Bed HH2b, Manuherikia River section, located 21.02–21.31 m above the base of the Bannockburn Formation, Central Otago, New Zealand.

Age Justification: The fossil horizon is assigned to the Altonian New Zealand Stage based on palynostratigraphical data (71), and we based the minimum age on the upper boundary of the Altonian Stage. Specifying a maximum age for the *Nestor*-*Strigops* divergence is challenging, because Nestoridae is endemic to New Zealand and there are very few non-penguin bird remains from sites older than the Bannockburn Formation. While it has been proposed that New Zealand was submerged in the Oligocene (72) and this event could be used as a maximum age constraint for endemic New Zealand clades, contradictory evidence suggests submergence was not complete and many terrestrial groups persisted in New Zealand through the Paleogene-Neogene boundary (e.g., 73). Thus, we abstained from hypothesizing a maximum age for this specific split and extended the maximum to 66.5 Ma, matching that used for the next deepest calibrated node, Psittacopasseres.

Calibration 5: Crown Acanthisittidae (split between *Acanthisitta* and *Xenicus*

Minimum Age: 15.9 Ma

Maximum Age: 56.0 Ma

Fossil Taxon: *Kuiornis indicator*

Specimen: NMNZ S.50929, tarsometatarsus

Reference: (74)

Phylogenetic Justification: Analyses of morphological data support a sister group relationship between *Kuiornis* and *Acanthisitta* (74). This relationship is retained when a molecular constraint is applied for extant taxa (75).

Locality: Bed HH4, Manuherikia River section, Central Otago, New Zealand. This bed is located 25.63–25.83 m above the base of the Bannockburn Formation, and 2.15–2.35 m above the top of a prominent bed of oncolites (70, 74).

Age Justification: The fossil horizon is assigned to the Altonian New Zealand Stage based on palynostratigraphical data (71), and so we based the minimum age on the upper boundary of the Altonian Stage. Specifying a soft maximum age for the *Acanthisitta* - *Xenicus* divergence is more problematic, because Acanthisittidae is endemic to New Zealand and few non-penguin bird remains are known from New Zealand sites older than the Bannockburn Formation. We therefore based the maximum on the maximum age of the early Eocene. The oldest stem Passeriformes date to the early Eocene, but there are no records of crown Passeriformes of any type in the Eocene, suggesting that the earliest divergence in the crown clade (one half of which gave rise to Acanthisittidae) had not yet occurred.

Calibration 6: Eupasseres (split between Suboscines and Oscines)

Minimum Age: 27.25 Ma

Maximum Age: 56.0 Ma

Fossil Taxon: Suboscines indet.

Specimen: SMF Av 504, articulated partial wing (carpals, carpometacarpus and phalanges)

Reference: (76)

Phylogenetic Justification: The presence of a distally protruding fingerlike process at the cranial edge of metacarpal III is an apomorphy supporting assignment of SMF Av 504 to at least the stem suboscine lineage (76). Additionally, the hatchet-shaped phalanx II-1 is similar to that of suboscines and differs from the shape seen in oscines, Acanthisittidae, and *Zygodactylus luberonensis*. This feature is potentially another apomorphy for suboscines, although its distribution has not been fully documented.

Locality: Luberon, southern France.

Age Justification: The exact horizon from which this specimen was collected was not specified, but the Luberon fossil deposits, as a whole, are considered to fall within the MP21-MP25 age range (76). We conservatively used the minimum age of MP25 as a hard minimum date (see Fig. 28.10 of 77). The oldest reported stem Passeriformes are from the early Eocene. Furthermore, no crown Passeriformes of any type are found in Eocene deposits such as the Green River Formation, Messel Formation, London Clay Formation, or Fur Formation, each of which otherwise preserves an abundance of small bird fossils. These deposits are all from the Northern Hemisphere. Eupasseres appear to have originated in the Southern Hemisphere, which has a much poorer fossil record for small birds. Nevertheless, several Oligocene-Miocene fossils of early diverging members of Eupasseres have been described from European deposits, which indicate that the clade was not entirely restricted to the Southern Hemisphere early in their evolution. These include the Oligocene fossils *Wieslochia weissi* (a possible stem suboscine or perhaps a lineage just outside Eupasseres; 78), a potential Miocene record of the suboscine lineage Eurylaimidae (79), and several Miocene tarsometatarsi that retain plesiomorphic features suggesting they represent an extinct lineage outside of Eupasseres (80). Thus, the potential for preservation of Eupasseres in the mid-Cenozoic of the Northern Hemisphere is demonstrated, and the early Eocene provides a conservative maximum.

Calibration 7: Split between *Atrichornis* and *Menura*

Minimum Age: 16.0 Ma

Maximum Age: 56.0 Ma

Fossil Taxon: *Menura tyawanoides*

Specimen: QM F.20887 (AR 11466), carpometacarpus

Reference: (81)

Phylogenetic Justification: The revised phylogenetic hypothesis presented in this manuscript places Atrichornithidae as sister to Menuridae. The overall body sizes of lyrebirds and scrub-birds differ greatly, with both species of extant *Menura* averaging close to 1kg, whereas extant *Atrichornis* falls between ~20g and 55g (82). This difference is reflected in the maximum length of the carpometacarpi of these taxa: *Atrichornis clamosus* exhibits a mean carpometacarpus length of 10mm, whereas the carpometacarpi of *Menura novaehollandiae* and *M. alberti* average 38.3mm and 36.3mm, respectively. The isolated carpometacarpus of *M. tyawanoides* exhibits a maximum length of 29.3 mm; although slightly shorter than the carpometacarpi of extant Menuridae, this greatly exceeds the size of any extant Atrichornithidae (81) and the vast majority of extant passerines. Aside from the considerable size difference between extant *Menura* and *Atrichornis*, the carpometacarpi of *Atrichornis* and *Menura* are quite distinct, with *M. tyawanoides* exhibiting the following characters listed by (83) as diagnostic for *Menura* with respect to *Atrichornis*:

1) Ligamental attachment of the pisiform process prominent.
2) External ligamental attachment prominent.
3) Carpometacarpus not stout as in *Atrichornis*.
4) Prominence present on metacarpal II about midway between proximal and distal ends on the external border.
5) The external carpal trochlea extends on slightly farther proximally than the internal trochlea.
6) Intermetacarpal tuberosity with relatively wide base when viewed externally.

Locality: Upper Site (System B), Riversleigh World Heritage Area, Queensland, Australia.

Age Justification: The principal fossil-bearing sites from this locality can be divided into three ‘systems’, with systems B and C yielding most fossil passerines. The site producing *M. tyawanoides* derives from the Upper Site of System B, which is interpreted as belonging to Faunal Zone B (early Miocene). Faunal Zone B is inferred to span 16–20 Ma based on biocorrelation (reviewed in ref. 84). Arena et al. (85) assigned the Upper Site specifically to B3, the youngest subdivision, based on refinement of regional biostratigraphy. Given this evidence, we used 16 Ma as the minimum age for this divergence. We based the maximum on the maximum age of the early Eocene. The oldest stem Passeriformes date to the early Eocene, but the Eocene lacks records of crown Passeriformes of any type, suggesting that the earliest divergence in the crown clade had not yet occurred.

Calibration 8: Split between Meliphagidae and Pardalotidae

Minimum Age: 14.22 Ma

Maximum Age: 56.0 Ma

Fossil Taxon: Meliphagidae indet.

Specimen: QM F20622, distal portion of tarsometatarsus

Reference: (86)

Phylogenetic Justification: The referral of this specimen to total-clade Meliphagidae is based on a suite of character states, including an enlarged canalis for M. flexor hallucis longus, a triangular-shaped trochlea metatarsi II, a large and deep fossa metatarsi I extending at least to the midline of the tarsometatarsus, and the medial side of trochlea metatarsi III projecting more than the lateral side (86). Although certain other Australasian taxa exhibit generally similar tarsometatarsi (including Pomatostomidae; 86), these taxa can be distinguished from Meliphagidae by the character suite above observable in QM F20622.

Locality: Middle Miocene Ringtail Site (87), Riversleigh World Heritage Area, Queensland, Australia.

Age Justification: The Ringtail site forms part of Riversleigh System C (88), and is thought to be of middle Miocene age based on species assemblage biocorrelation (87–90). The Model 1 isochron equilibrium age obtained for this site by Woodhead et al. (84) corresponds to 13.56 Ma ± 0.66 Ma; thus, we used a minimum age of 14.22 Ma for this specimen. We based the maximum on the maximum age of the early Eocene. The oldest stem Passeriformes date to the early Eocene (and include records from Australia) but the Eocene lacks records of crown Passeriformes of any type, suggesting that the earliest divergence in the crown clade had not yet occurred.

Calibration 9: Split between *Orthonyx* and *Pomatostomus*

Minimum Age: 17.72 Ma

Maximum Age: 56.0 Ma

Fossil Taxon: *Orthonyx kaldowinyeri*

Specimen: QM 56329 near-complete right tarsometatarsus

Reference: (91)

Phylogenetic Justification: Following (92), the fossil tarsometatarsi recovered from the Oligo-Miocene localities at Riversleigh can be referred to *Orthonyx* on the basis of the following apomorphies:

1) The impressio ligamentum collateralis lateralis low but very large.
2) The plantar surface immediately proximal to the incisura intertrochlearis lateralis deeply excavated, whereas the plantar surface immediately proximal to the incisura intertrochlearis medialis very shallowly excavated.

The referral of these tarsometatarsi to *Orthonyx* is additionally supported by a diagnostic combination of character states, enumerated by (92).

Locality: Neville's Garden Site, Riversleigh World Heritage Area, Queensland, Australia.

Age Justification: Neville's Garden Site represents Faunal Zone B at Riversleigh. This site represents an area of cave deposits comprising both karst formations and a pool deposit (84). Two U/Pb radiometric dates (17.85 ± 0.13 Ma vs 18.24 ± 0.29 Ma) from Neville's Garden Site are associated with speleothems that include flowstones wrapping around fossils (84). These stalagmites are interpreted as contemporary in age with the fossils, and we used the youngest possible date, inclusive of error, for a minimum age calibration of 17.72 Ma. Future work may consider a stratigraphically older specimen referred to *O. kaldowinyeri*, which is less complete and less confidently referred. This specimen, QM F30244, comes from the Hiatus Site at Riversleigh, and comprises a distal right tarsometatarsus. The precise age of the Hiatus Site remains poorly constrained. The Hiatus Site represents 'Faunal Zone A', which has been interpreted as late Oligocene based on biocorrelation, stratigraphy, and multivariate studies of more than 200 local faunas at Riversleigh (87–90, 92–94). Based on biocorrelation to the faunas from the Etadunna and Namba Formations in South Australia (90), we applied a minimum age matching the top of Chron 7r, with the numerical date (24.74 Ma) selected from Table 28.2 of (77). This is a conservative minimum and the age may prove older. Attempts to directly date the Hiatus Site have been unsuccessful thus far (84). We base the maximum on the maximum age of the early Eocene. The oldest stem Passeriformes date to the early Eocene but the Eocene lacks no records of crown Passeriformes of any type, suggesting that the earliest divergence in the crown clade had not yet occurred.

Calibration 10: Stem *Daphoenositta* (split between *Daphoenositta* and *Mohoua*)

Minimum Age: 11.6 Ma

Maximum Age: 56.0 Ma

Fossil Taxon: *Daphoenositta trevorworthyi*

Specimen: QM F57897, distal left tibiotarsus

Reference: (95)

Phylogenetic Justification: QM F57897 was referred to *Daphoenositta* of the monogeneric Neosittidae (sittellas) by (95) based on a diagnostic combination of character states including:

1) Distal margin of pons supratendineus located proximally of condylus medialis by a distance about equal to a third of condyle length.
2) Lateral and medial bony ridges for attachment of retinaculum m. fibularis long and low.
3) Bony ridges for retinaculum m. fibularis about distally level with tuberositas retinaculi extensoris lateralis.
4) Tuberositates retinaculorum extensorium elongate.

Locality: Rick's Sausage Site, Faunal Zone C deposits, Riversleigh World Heritage Area, Queensland, Australia.

Age Justification: Rick's Sausage Site is not precisely dated but is regarded as middle Miocene in age (85, 88, 94, 96) and assigned to Faunal Zone C on the basis of stage-of-evolution biocorrelation. Our recommended minimum age accommodates uncertainty in the age of the upper part of this zone, and is placed at 11.6 Ma (84). We based the maximum on the maximum age of the early Eocene. The oldest stem Passeriformes date to the early Eocene but the Eocene lacks records of crown Passeriformes of any type, suggesting that the earliest divergence in the crown clade had not yet occurred.

Calibration 11: Crown Cracticidae (split between *Peltops* and (*Cracticus* + *Strepera*))

Minimum Age: 14.5 Ma

Maximum Age: 56.0 Ma

Fossil Taxon: *Kurrartapu johnnguyeni*

Specimen: QM F56251, tarsometatarsus

Reference: (97)

Phylogenetic Justification: Nguyen et al. (98) identified a unique apomorphy uniting *Kurrartapu* with *Cracticus* + *Strepera.* Incomplete ossification of the retinaculum extensorium tarsometatarsi is not observed in any other passerine group except the *Strepera*-*Cracticus* clade; thus, the fossil can be placed at least as the sister of these two extant taxa with confidence, despite the limited material.

Locality: Price is Right Site, Riversleigh World Heritage Area, northwestern Queensland, Australia.

Age Justification: The Price is Right Site has been interpreted as belonging to Faunal Zone B (early Miocene). However, a review of regional biostratigraphy by Woodhead et al. (84) found this site to be one of the more poorly constrained Riversleigh localities, with the possible range of ages encompassing the upper part of Faunal Zone B (B2 or B3) as well as the lower part of Faunal Zone C (C1). We thus used the estimated upper age boundary of lower Faunal Zone C (14.5 Ma: figure 6 of ref. 84) as a minimum age. Cracticidae are restricted to Australia, New Guinea, New Zealand and surrounding islands. Given the sparse record of pre-Miocene landbirds from this region, it is difficult to set a maximum date that accounts for the possibility of non-preservation. The earliest representative of the Cracticidae is an indeterminate scapula from the Miocene St Bathans Fauna (97) which is only slightly older than QM F56251. Probable stem Passeriformes date to the early Eocene in Australia, but the Eocene lacks records of crown Passeriformes of any type. Thus, the early Eocene is a conservative maximum.

Calibration 12: stem *Ammodramus* (split between *Ammodramus* and other sparrows)

Minimum Age: 7.5 Ma

Maximum Age: 18.6 Ma

Fossil Taxon: *Ammodramus hatcheri* (=*Paleostruthus hatcheri*)

Specimen: USNM 6647, rostrum

Reference: (99)

Phylogenetic Justification: Steadman (99) considered USNM 6647 to be more closely related to *Ammodramus savannarum* than other sparrows based on a combination of six characters:

1) Crista tomialis slightly concave in ventral aspect.
2) Os premaxillare tapering abruptly, with anterior tip very sharp.
3) Os premaxillare shallow in lateral aspect, with no distinct bend in the medial os nasale.
4) Nares large, rounded anteriorly.
5) Posterior border of ventral surface of os premaxillare only slightly anterior to junction of lateral os nasale and os maxillare.
6) Medial groove on ventral surface of os premaxillare distinct, but not deep.

We concur that the observable morphology closely resembles that of extant *Ammodramus* and differs from other closely related emberizids.

Locality: Quarry E of the Long Island local fauna sites, Phillips County, Kansas, USA.

Age Justification: An age of Hh1 (early Hemphilian) was established for Long Island Quarry (100). This mammal age spans 7.5-9.0 Ma (77: Fig. 29.9). Thus, we used 7.5 Ma for the hard minimum age. Although the fossil record of sparrows is poor, the regional record of passerines provides the context for formulating a maximum age. The fossil record of crown Passeriformes in North America is shallow. Aside from *Ammodramus hatcheri*, only a handful of Miocene songbird fossils have been reported including *Palaeoscinis turdirostris* (101), *Miocitta galbreathi* (102), and several still undescribed fossils from the Truckee Formation (57). The oldest reported North American songbirds are putative records of Parulidae from the early Miocene (Hemingfordian) Thomas Farm locality, which remain undescribed (68). This distribution suggest New World sparrows had not originated prior to the Miocene. We used the upper age boundary of the Hemingfordian (18.6 Ma; 77: Fig. 29.9), which conservatively encompasses all North American passerine records, as a maximum.

Calibration 13: Split between Regulidae and Certhioidea

Minimum Age: 17.2 Ma

Maximum Age: 56.0 Ma

Fossil Taxon: *Certhiops rummeli*

Specimen: NMA 2007/51/2021, tarsometatarsus

Reference: (103)

Phylogenetic Justification: The phylogenetic hypothesis presented here corroborates the finding that Certhioidea comprises *Tichodroma*, *Sitta*, and *Certhia*+*Salpornis* as successive hierarchical sisters to a Troglodytidae+Polioptilidae clade. This topology suggests that wrens and gnatcatchers may be descended from antecedents that exhibited a scansorial ecology, as well as numerous hindlimb specializations related to such a lifestyle. The morphology of the tarsometatarsus of *Certhiops rummeli* does not allow a clear assessment of its immediate extant sister group (although it exhibits 7 distinct apomorphies shared with climbing members of the Certhioidea), and it is conceivable that the fossil could represent an early stem group relative of *Tichodroma*, *Sitta*, *Certhia*+*Salpornis*, the Troglodytidae + Polioptilidae clade, or the most exclusive clade bracketed by *Tichodroma* and Troglodytidae. However, the clear mosaic of 'climbing certhioid' character states exhibited by the tarsometatarsus of *Certhiops rummeli* allows confident placement of the fossil somewhere within this broader radiation.

These character states are as follows (from ref. 103):

1. Crista lateralis hypotarsi reaches farther proximally than the crista medialis hypotarsi, almost protruding beyond the eminentia intercotylaris. In other passerines, the crista lateralis hypotarsi does not protrude.
2. The hypotarsal canals for the deep flexor tendons are characteristically arranged: The diameter of the canal for the fpp3-tendon is markedly smaller than the diameter of the single canal for the fp3- and fp4-tendons. This size difference is obvious in the fossil even though the fpp3-canal is confluent with the canals for the fp2- and fpp2- tendons. The fp3,fp4-canal lies more plantarly with respect to the fpp3-canal. In other passerines, the fpp3-canal is on the same level as the fp3,fp4-canal and both are of similar diameter.
3. In the fossil specimen as well as in *Tichodroma* and *Certhia*, the fp3,fp4-canal is incompletely ossified and forms a shallow, plantarly open furrow. In *Sitta*, however, the canal is completely ossified, as is the case in the majority of Eupasseres (80).
4. Shaft with triangular medial extension just distal to fossa metatarsi I that is comparatively smooth in *Tichodroma muraria* [A similar structure is also present in wrens (Troglodytidae), tits (Paridae), and honeyeaters (Meliphagidae; 86)].
5. The trochleae metatarsorum II–IV are proximodistally short and separated from each other by broad incisurae intertrochleares.
6. The trochlea metatarsi III bears a deep trochlear furrow. This furrow is especially deep in *Certhia*.
7. The trochlea metatarsi III is large and protrudes dorsally as well as plantarly. In both *Certhiops* and *Tichodroma*, the lateral rim of this trochlea is smaller than the medial one, while both rims are of almost equal size in extant nuthatches and treecreepers.

As such, we recommend the fossil be used to minimally constrain the age of origin of the Certhioidea (i.e., the divergence between Regulidae and Certhioidea).

Locality: Petersbuch 62 fissure filling, north of Eichstätt, Germany.

Age Justification: Some uncertainty exists regarding the precise stratigraphic age of this specimen. Manegold (103) describes the type locality as Petersbuch 62, a karstic fissure filling north of Eichstätt, which is assigned to Mammal Neogene Zone 3 based on biostratigraphy (MN 3; early Miocene) and is thought to be roughly contemporaneous with the nearby 20.5–18 Ma Wintershof West site (104, 105); however, future work should be devoted to clarifying the stratigraphic age of the Petersbuch 62 locality. Based on the assignment of the locality to MN3, we assigned a minimum age corresponding to the upper boundary of MN2 of 17.2 Ma (77: Fig. 29.9). We based the maximum on the maximum age of the early Eocene. The oldest stem Passeriformes date to the early Eocene but the Eocene lacks records of crown Passeriformes of any type, suggesting that the earliest divergence in the crown clade had not yet occurred.

Detailed phylogenetic results

Our results establish relationships in a number of clades that have been difficult to resolve, such as the Old World suboscines (infraorder Eurylaimides), tyrant flycatchers and allies (parvorder Tyrannida), and superfamily Malaconotoidea (Fig. 1). Our results also clarify relationships within the parvorders Sylviida, Muscicapida, and Passerida, although a few nodes in these clades remain difficult to resolve owing to rapid splitting of lineages. For instance, our analyses clarify the branching order of the most distant lineages in parvorder Sylviida although relationships among the superfamilies Locustelloidea, the clade comprising the superfamilies Sylvioidea and Aegithaloidea, and the families of wren-babblers (Pnoepygidae) and swallows and martins (Hirundinidae) remain unclear in all analyses. In the parvorder Muscicapida, the relationships among the superfamilies Bombycilloidea, Muscicapoidea, Certhioidea, and the family of kinglets (Regulidae) remain ambiguous, although relationships within each superfamily are now clarified, with the exception of Bombycilloidea. Within Bombycilloidea, the relationships among the families of palmchat (Dulidae), waxwings (Bombycillidae), silky-flycatchers (Ptiliogonatidae), and hylocitrea (Hylocitreidae) are consistent across all analyses (Figs. S1–S5). However, we were unable to resolve the positions of the extinct Hawaiian honeyeaters (Mohoidae) and hypocolius (Hypocoliidae) in Bombycilloidea (Figs. S1–S5, Supplementary File S2), likely because of limited sequence data collected from these two families (Supplementary File S1). In parvorder Passerida, we resolved the branching order of lineages with the exception of two sections of this clade. The first section involves relationships among Przevalski's finch (Urocynchramidae), the clade comprising the three families of weavers (Ploceidae), estrildid finches (Estrildidae), indigobirds and wydahs (Viduidae), and the rest of the families of Passerida. The second section of Passerida that remains difficult to disentangle involves the placement of the Caribbean genera of chat-tanagers (*Calyptophilus*) and wrenthrush (*Zeledonia*).

Our phylogenetic analyses also uncovered a number of new relationships among three enigmatic Afrotropical species (53, 106) and recently proposed passerine families. Two of the African endemics, the green hylia *Hylia prasina* and the tit hylia *Pholidornis rushiae*, formed a clade within the superfamily Aegithaloidea (Fig. 2). Support for this sister relationship was previously found using molecular data (107), but the phylogenetic position of this clade remained unclear (107, 108). We found that *Hylia* and *Pholidornis* are sister to a clade formed by long-tailed tits (Aegithalidae) and bush warblers and allies (Scotocercidae). These results support the recognition of the family Hyliidae Bannerman, 1923, comprising the genera *Hylia* and *Pholidornis,* as previously suggested based on other data (107–109). We were also able to place another Afrotropical endemic, Grauer's warbler *Graueria vittata,* as sister to the reed-warblers (Acrocephalidae) in the superfamily Locustelloidea, and our results suggest that this lineage diverged from other members of Acrocephalidae ~17 Ma. Among families with uncertain relationships, we resolved the recently described monotypic family of the spotted elachura (Elachuridae; 110) as sister to the superfamily Muscicapoidea. Finally, our results support the recognition of several additional recently-recognized passerine families, including Platylophidae, Hylocitreidae, Tichodromidae, Salpornithidae, and Chloropseidae (106, 111) to maintain monophyly of families (Tichodromidae, Salpornithidae) or to acknowledge the deep divergence between these families (Platylophidae, Hylocitreidae, Chloropseidae) and their closest relatives.

Our results support the grouping of eight families in Corvides into a clade (Orioloidea), which was previously reported in a study that used genome-wide loci (25): whipbirds and wedgebills (Psophodidae), ploughbill (Eulacestomatidae), shriketits (Falcunculidae), Australo-Papuan bellbirds (Oreoicidae), painted berrypeckers (Paramythiidae), shrike-babblers and vireos (Vireonidae), whistlers (Pachycephalidae), and orioles (Oriolidae). As in ref. (25), relationships among Psophodidae, Eulacestomatidae, the clade formed by Falcunculidae and Oreoicidae, and the clade formed by the four other families remain uncertain even though we sampled different individuals with longer sequences. Within superfamily Corvoidea, the family of fantails (Rhipiduridae) and drongos (Dicruridae) are successive sister taxa to the rest of the superfamily, which form a clade. Within this clade, however, relationships among monarchs (Monarchidae), ifrit (Ifritidae), birds of paradise (Paradisaeidae), Australian mudnesters (Corcoracidae), melampittas

(Melampittidae), and the clade formed by shrikes (Laniidae), crested jay (Platylophidae), and crows and jays (Corvidae) are unclear.

In a previous study of songbirds (25), the sister relationship of the families of fairy bluebirds (Irenidae) and leafbirds (Chloropseidae) was uncertain. Sampling two species in each family has improved support for this sister relationship. We doubt whether denser taxonomic sampling in unresolved passerine clades will clarify some of the remaining recalcitrant nodes because a number of these difficult nodes involve monotypic families (e.g., Eulacestomatidae, Ifritidae) or are fairly well-sampled in this study (e.g., Sylviida, Corvoidea). That said, additional sequence data may clarify the phylogenetic position of Urocynchramidae, Hypocoliidae, and the extinct Mohoidae. Although we recovered sequence data from thousands of UCE loci for each of the specimens representing these three families, these sequence data were derived from museum skin specimens and were much shorter, on a locus-by-locus basis, than the average (Supplementary File S1). Sampling a different type of sequence data in concert with UCEs, such as protein-coding genes and introns, may also help to place recalcitrant nodes in passerine phylogeny.

Comparison of biogeographic results from alternative models

Biogeographic analyses including stem passerines and other fossil taxa (Figs. S7, S8) yield an Australo-Pacific origin of crown passerines across all six different possible phylogenetic configurations of fossil taxa under the DEC + *j* model (Fig. S7), as well as under two of these configurations with the DEC model (Fig. S8). Analyses of the four remaining phylogenetic configurations of fossils under the DEC model suggest an ancestral area of Eurasia + Australo-Pacific region for passerines (Fig. S8), but we consider this to be a geographically unrealistic scenario because the two land masses were separated by thousands of kilometers during the middle Eocene (112).

Biogeographic reconstructions under the DEC + *j* model suggest a Eurasian origin of crown suboscines (Tyranni, Fig. 1) and a North/Central American origin of crown New World suboscines (Tyrannides; Fig. 1), no matter the position of fossil taxa (Fig. S7). However, our DEC results are equivocal, suggesting either a Laurasian (North American + Eurasia) or a Laurasian + South American origin of crown suboscines, depending on the placement of the early Oligocene fossil taxon *Wieslochia* (Fig. S8).

Our DEC + *j* results unequivocally suggest crown Old World suboscines (Eurylaimides) originated in Eurasia, regardless of the position of fossil taxa (Fig. S7). On the other hand, our DEC results suggest crown Eurylaimides originated in North America, Eurasia, Africa, and Australasia in five configurations of fossil taxa, but yield a North America, Eurasia, and Africa origin in one configuration (Fig. S8).

Diversification rate shifts: Comparison with Jetz et al. (113)

To better understand the differences we observed between our study and the results of Jetz et al. (113), we analyzed a subset of the Jetz et al. (113) data using our methodological approach. We drew a random set of 100 Stage 2 trees from the posterior generated by Jetz et al. (113) using the Hackett et al. (114) backbone and extracted the passerine portion of each tree. Using the same methods described for analysis of the UCE tree (aside from random tip addition), we analyzed diversification rate on this posterior of trees in order to estimate the distribution of rate shifts and branches with the highest marginal likelihood of a shift for each. To summarize these data across the posterior of topologies, using BAMMtools we: a) extracted the minimum number of inferred events for each topology, b) estimated the marginal odds of a rate shift occurring at each branch in each topology, c) extracted the *n* clades with the highest probability of a rate shift for each topology (where *n* is the average minimum number of events across all topologies), and d) counted the frequency of each shifted clade across the posterior. We then compared the top *n* most

frequently recovered clades to those previously reported by Jetz et al. (113) and the results obtained in this study.

Analyses of the Jetz et al. (113) data with BAMM inferred an average of 22.0 (mean range from 15.0–31.7) rate shifts across the passerine tree. This average is substantially lower than might be expected given results from analyses of our data, which yielded a range of 14–25 events on the UCE backbone tree alone (i.e. excluding shifts within groups). Based on this result, we extracted the 15 clades with the highest marginal odds ratio of a rate shift from analyses of each posterior tree, then counted the frequency with which a shift was identified in each clade across trees. Clades with rate shifts occurred an average of 3.1 times across the set of 100 posterior trees, with a range from 1 to 88. That is, no single rate shift was found with high marginal odds across the entire posterior of trees and only four were found in more than half of all trees from the posterior.

The results for the 15 clades with the highest frequencies (all highly ranked in >15% of the posterior) are summarized in Table S2. Five (clades 5, 7, 8, 10, and 15) of the 15 groups consistently identified with a rate shift were not sampled by our UCE tree. Three of these clades (5, 7, and 10) are variants of the same group (the Darwin's finches and allies), indicating significant uncertainty regarding the precise placement of the rate shift within this group. The other two groups are the *Sporophila* seedeaters (previously recognized as an extraordinary radiation, 115), and the cardueline finches. Of the remaining 10 clades identified, four are monophyletic whereas six are paraphyletic in our analyses. Of the four rate-shifted groups that are monophyletic in our analyses, we inferred corresponding rate shifts for three: clade 1 (Furnariidae + Dendrocolaptidae), clade 3 (Thamnophilinae), and clade 14 (Tyrannidae excluding Hirundineinae). The fourth rate shift, in clade 12 (Emberizoidea plus Fringillidae and Motacillidae), was not found in the UCE tree. Finally, of the six rate-shifted clades that are paraphyletic on our tree, four correspond roughly to clades that are found in our analyses, with some of the conflicts caused by single problematic taxa (e.g., placement of *Elachura* with sylvioids based on taxonomy versus its likely relationship to muscicapoids based on data reported here). We found roughly corresponding rate shifts on the UCE tree for three of these (clades 6, 9, and 11). For the fourth (clade 2), we found three rate shifts nested within the corresponding clade. The fifth (clade 4) differed so substantially in composition from our best estimate of passerine phylogeny that we hesitate to conclude that our results were based on the same underlying biological signal. The sixth (clade 13, including the rapidly diversifying white eyes) may not have been identified in our analyses due to the sparsity of our taxon sampling in that region of the tree.

It is important to note that many of the rate shifts identified in these BAMM analyses were not identified by Jetz et al. (113): of the 13 likely independent shifts we identified in our BAMM analyses of the Jetz et al. (113) data (i.e. excluding two alternative definitions of the Darwin's finch clade), fewer than half were reported by Jetz et al. (113). Conversely, our analyses recovered fewer than half of the 14 rate shifts originally reported by Jetz et al. (113) from analyses of these same trees. This strongly suggests that differences in analytical approach (i.e., MEDUSA versus BAMM) contribute significantly to the differing results obtained from their analyses and those we report based on our UCE tree. However, we also note that there is substantial variation in inferred rate shifts across the posterior of trees, and both phylogenetic and branch length uncertainty contribute significantly to the contrasting results that we observed between our analysis of UCE data using BAMM and those results originally reported by Jetz et al. (113). In particular, we have been generous in interpreting shifts on the two sets of trees as representing the same underlying biological signal despite phylogenetic conflicts (in some cases substantial) between the two.

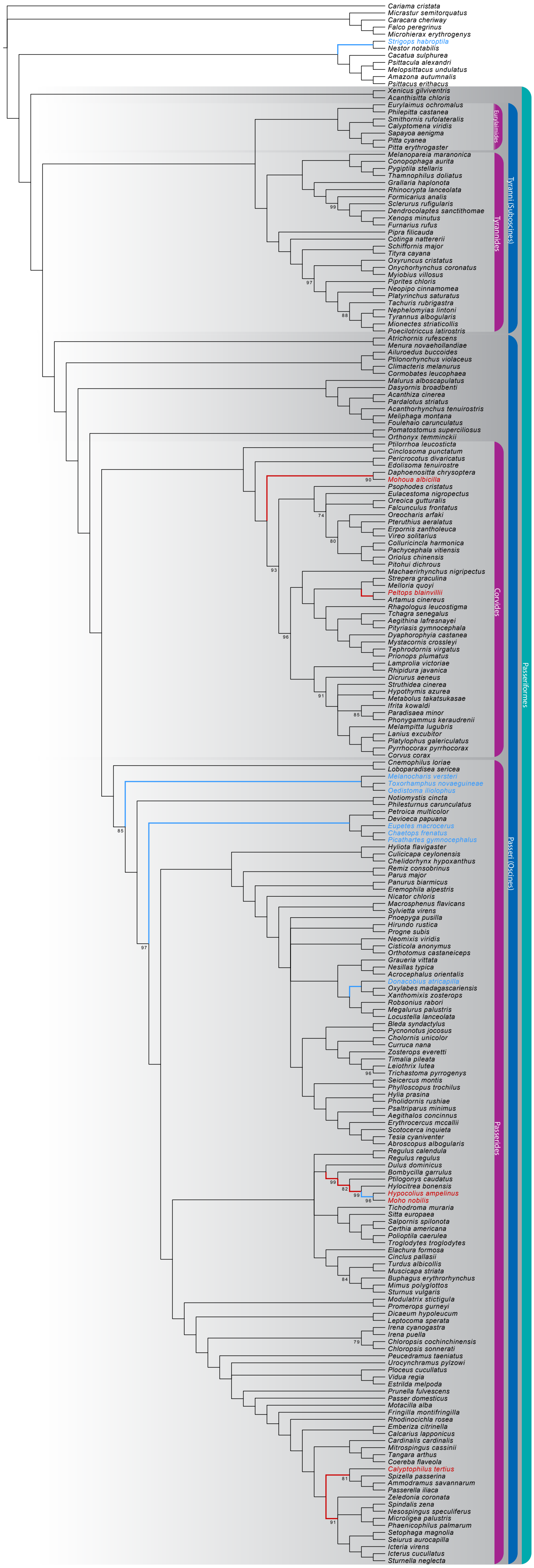

Fig. S1. Maximum likelihood estimate of phylogenetic relationships among passerine families. Bootstrap support (BS) values are 100% unless indicated at the node. Branches with < 70% BS are collapsed. Branches highlighted in red have highly supported (> 70% BS) conflicting topologies in all coalescent analyses (SVDQuartets, ASTRAL, ASTRID, STEAC), whereas those highlighted in blue have highly supported conflicting topologies in some but not all coalescent analyses. The taxa involved in highly supported conflicting topologies are highlighted in a similar fashion.

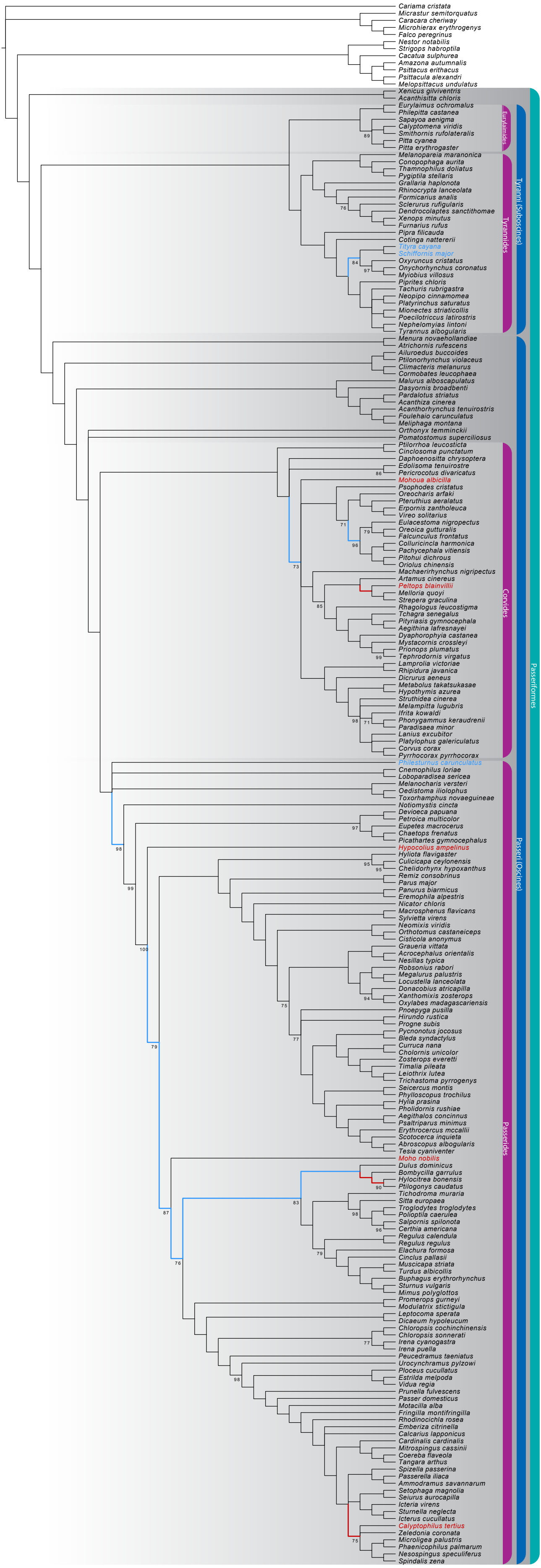

Fig. S2. Phylogenetic relationships among passerine families estimated using SVDQuartets. Bootstrap support (BS) values are 100% unless indicated at the node. Branches with < 70% BS are collapsed. Colored branches have a highly supported (> 70% BS) conflict with the maximum likelihood topology (Fig. S1) when analyzed with the full set of taxa. When analysis of subsampled and trimmed alignments (see Methods; Supplementary Files F2, F3) eliminated the highly supported conflict, the branch is blue; otherwise, the branch is red. The taxa involved in highly supported conflicting topologies are highlighted in a similar fashion.

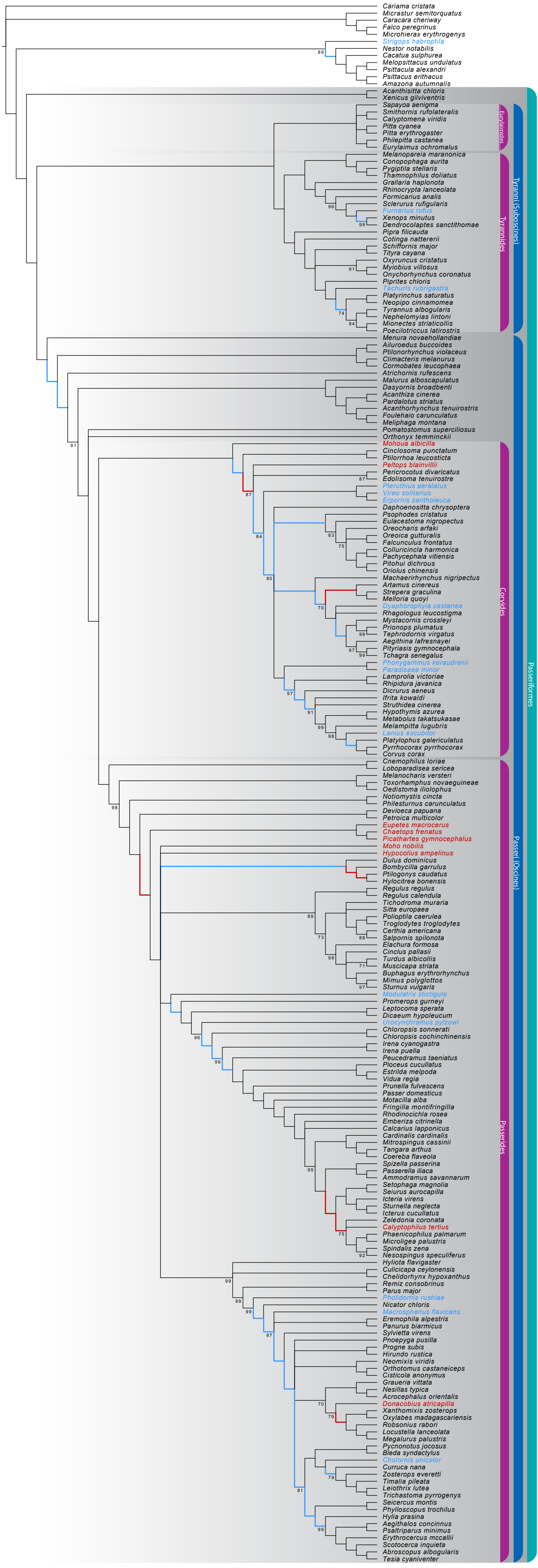

Fig. S3. Phylogenetic relationships among passerine families estimated using ASTRAL. Bootstrap support (BS) values are 100% unless indicated at the node. Branches with < 70% BS are collapsed. Colored branches have a highly supported (> 70% BS) conflict with the maximum likelihood topology (Fig. S1) when analyzed with the full set of taxa. When analysis of subsampled and trimmed alignments (see Methods; Supplementary Files F2, F3) eliminated the highly supported conflict, the branch is blue; otherwise, the branch is red. The taxa involved in highly supported conflicting topologies are highlighted in a similar fashion.

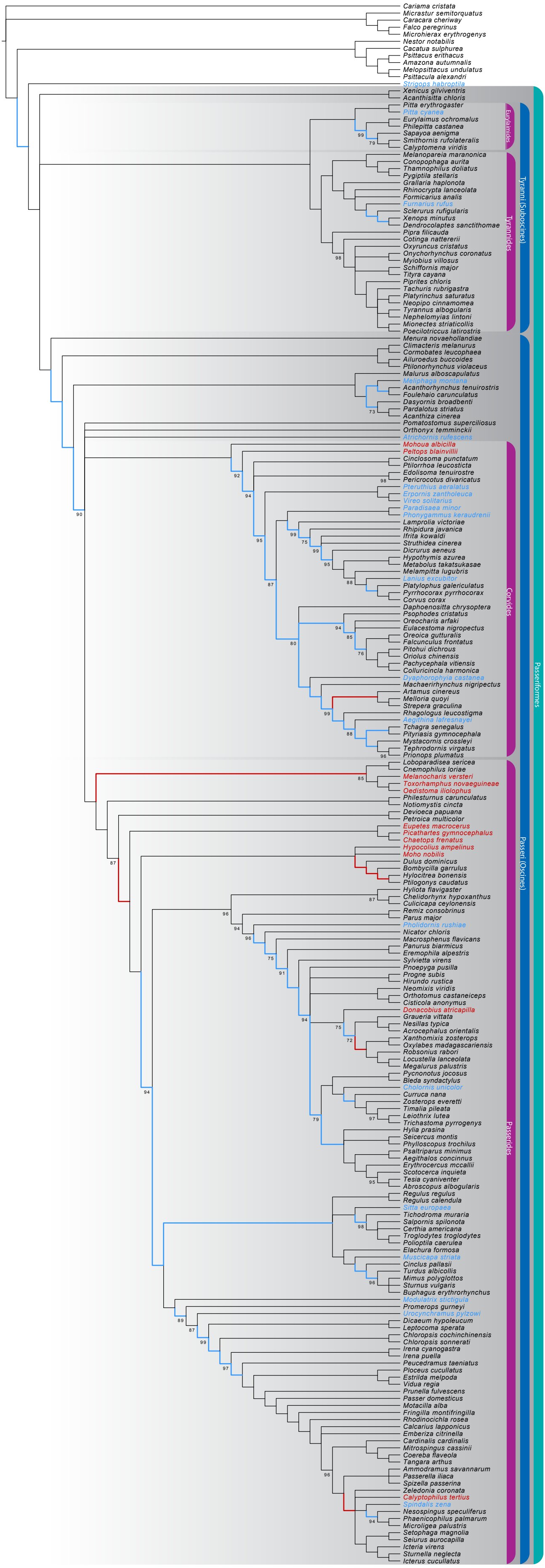

Fig. S4. Phylogenetic relationships among passerine families estimated using ASTRID. Bootstrap support (BS) values are 100% unless indicated at the node. Branches with < 70% BS are collapsed. Colored branches have a highly supported (> 70% BS) conflict with the maximum likelihood topology (Fig. S1) when analyzed with the full set of taxa. When analysis of subsampled and trimmed alignments (see Methods; Supplementary Files F2, F3) eliminated the highly supported conflict, the branch is blue; otherwise, the branch is red. The taxa involved in highly supported conflicting topologies are highlighted in a similar fashion.

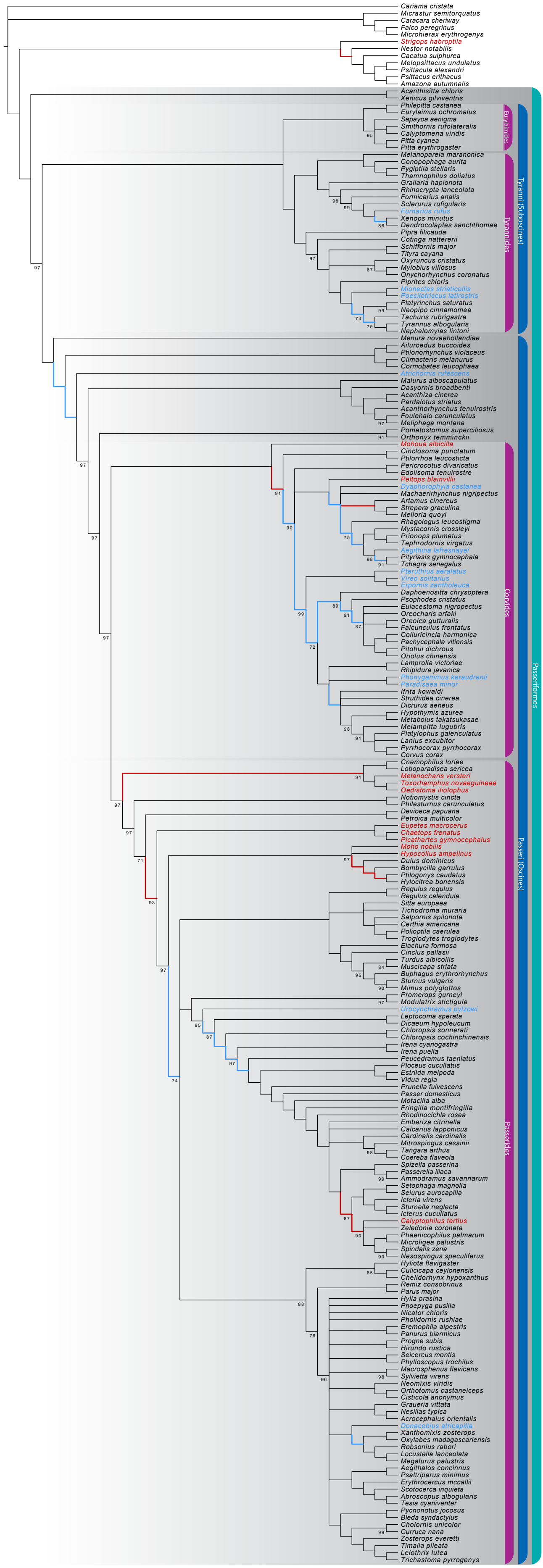

Fig. S5. Phylogenetic relationships among passerine families estimated using STEAC. Bootstrap support (BS) values are 100% unless indicated at the node. Branches with < 70% BS are collapsed. Colored branches have a highly supported (> 70% BS) conflict with the maximum likelihood topology (Fig. S1) when analyzed with the full set of taxa. When analysis of subsampled and trimmed alignments (see Methods; Supplementary Files F2, F3) eliminated the highly supported conflict, the branch is blue; otherwise, the branch is red. The taxa involved in highly supported conflicting topologies are highlighted in a similar fashion.

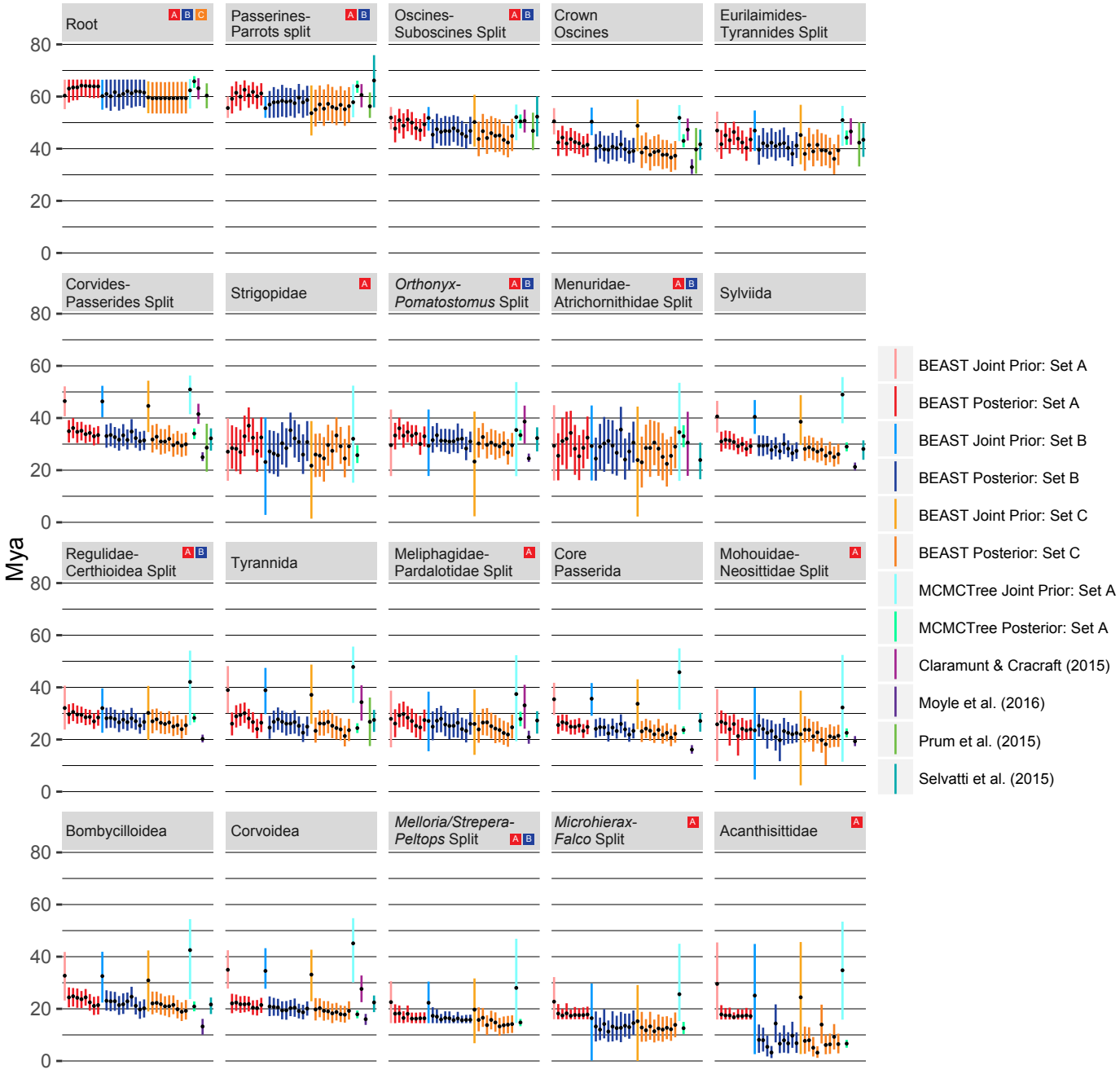

Fig. S6. Comparison of date estimates of key nodes in passerine phylogeny across three fossil calibration schemes (Sets A–C; see Methods for detailed description) using uniformly distributed priors. Bars represent 95% credible intervals of joint priors (MCMC without data) and posteriors of random samples of 25 loci. Color boxes in heading for each node indicate the set/s of calibrations in which the node was used as a calibration point. Date estimates from previous studies (25, 30, 32, 33) for the same node are also shown, if available.

Fig. S7. Comparison of date estimates of key nodes in passerine phylogeny across two locus-sampling schemes (random samples of 25 loci vs. 25 of most clock-like loci chosen using SortaDate), two choices of age maximum for fossil calibration priors (56 Ma vs. 80 Ma), and two fossil calibration schemes (Sets A and C) using lognormally distributed priors (see Methods for detailed description). Bars represent 95% credible intervals of joint priors (MCMC without data) and posteriors of age estimates. Color boxes in heading for each node indicate the set/s of calibrations in which the node was used as a calibration point. Date estimates from previous studies (25, 30, 32, 33) for the same node are also shown, if available.

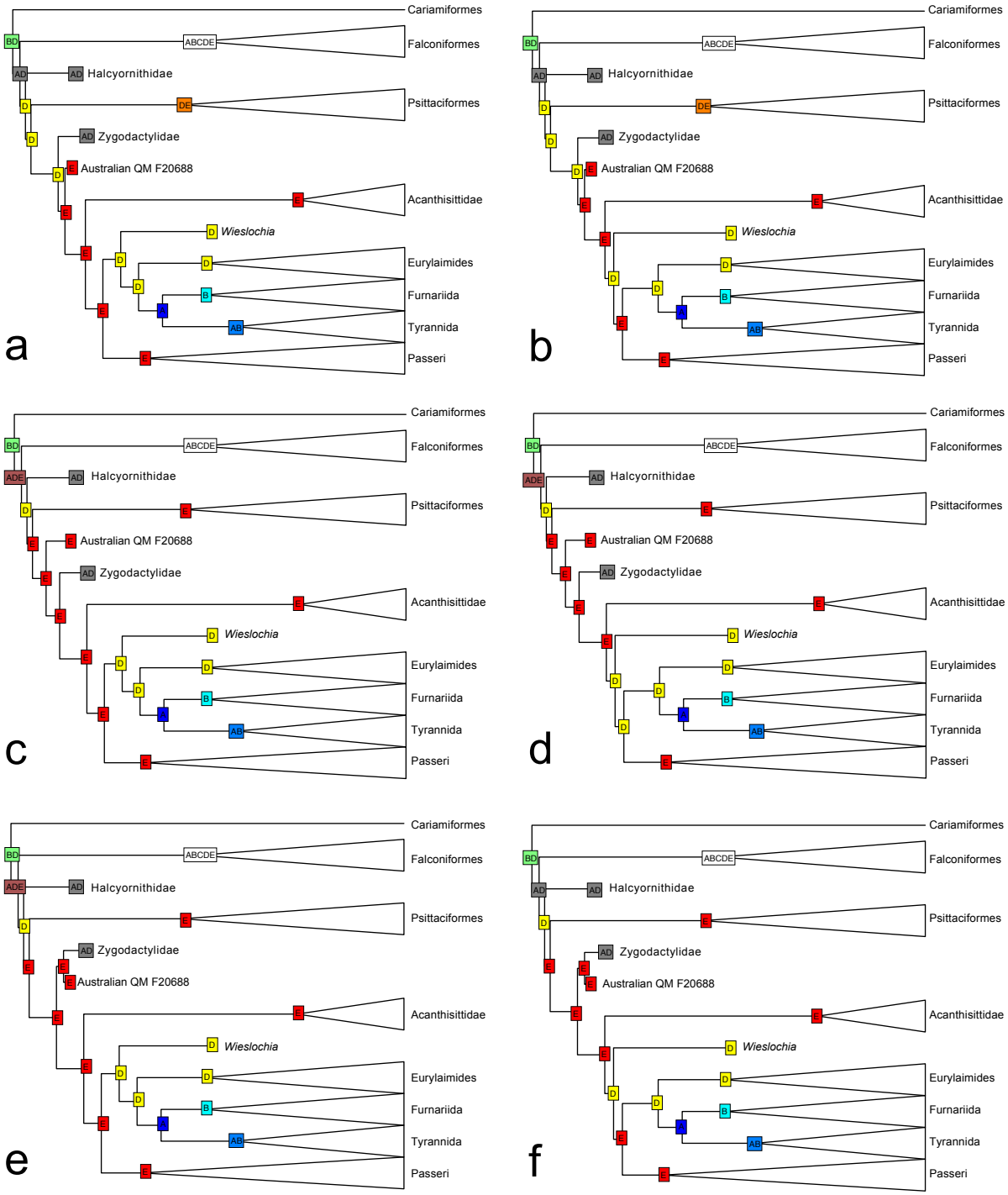

Fig. S8. Biogeographic reconstructions of major passerine lineages using the DEC + j model in BioGEOBEARS with the placement of fossil branches modified across the possible phylogenetic positions of fossil taxa Weislochia and Australian QM F20688 (a–f). Areas are defined as in Figs. 1–2 (A: North and Central America; B: South America; C: Africa; D: Eurasia; E: Australo-Pacific).

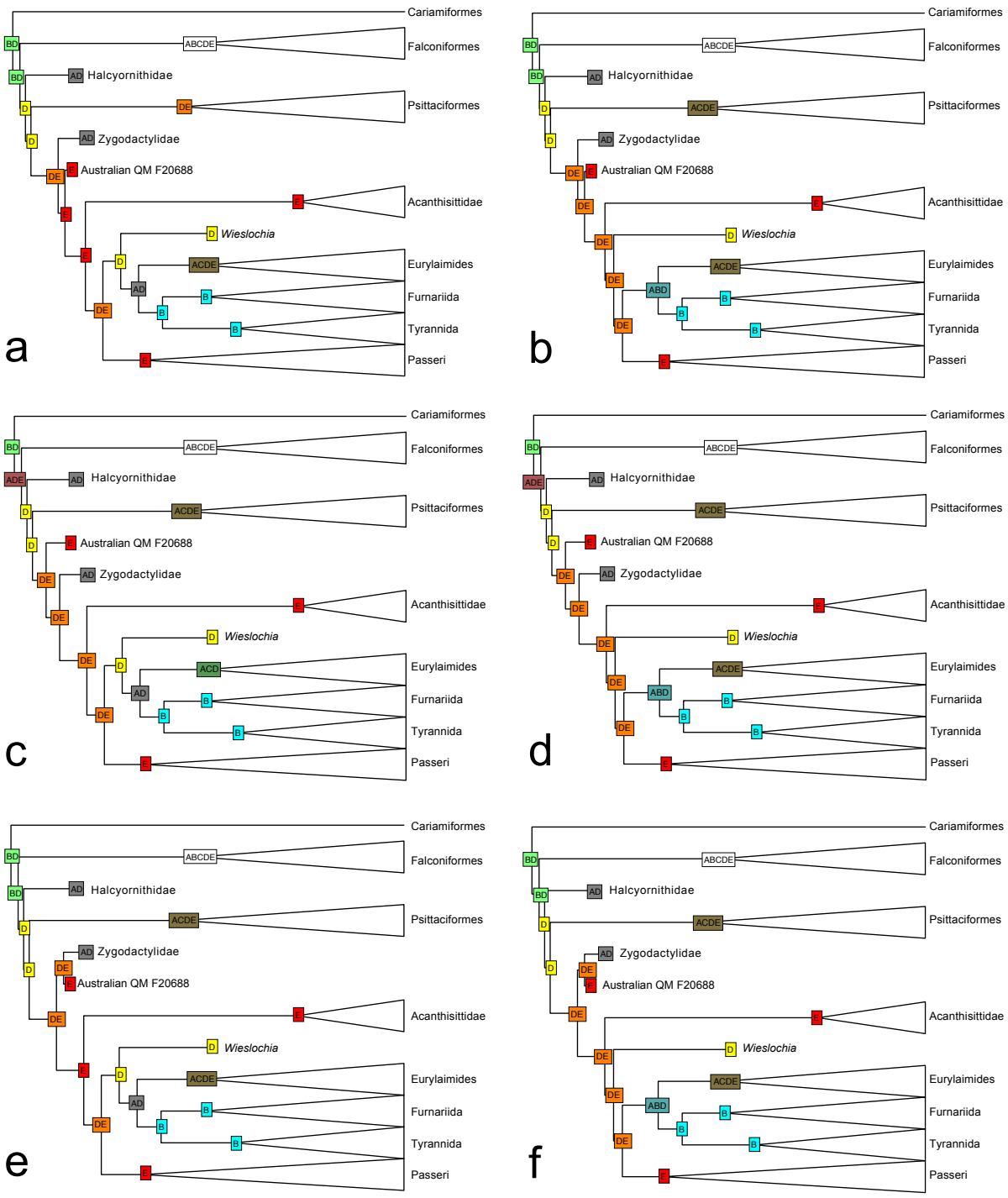

Fig. S9. Biogeographic reconstructions of major passerine lineages using the DEC model in BioGeoBEARS with the placement of fossil branches modified across the possible phylogenetic positions of fossil taxa Weislochia and Australian QM F20688 (a–f). Areas are defined as in Figs. 1–2 (A: North and Central America; B: South America; C: Africa; D: Eurasia; E: Australo-Pacific).

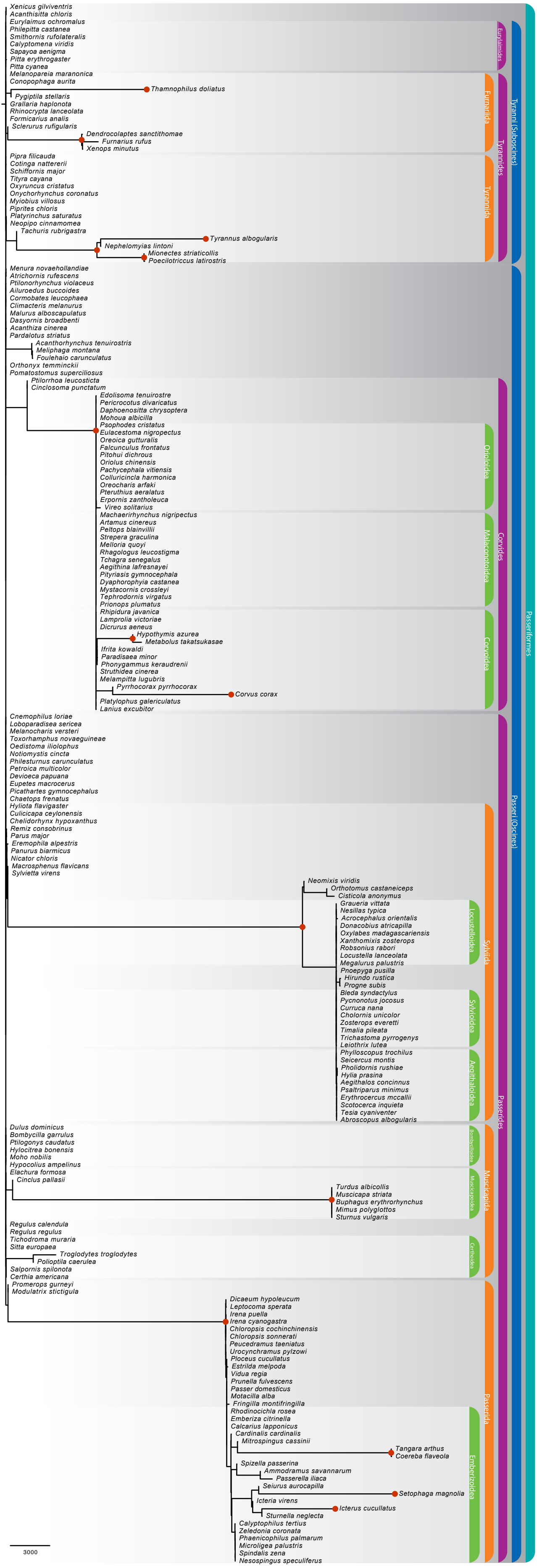

Fig. S10. Median marginal odds ratios for each branch of the passerine tree across BAMM analyses of 100 replicate trees. The 14 branches with the strongest evidence of rate shifts are highlighted with red circles at their descendant node.

Table S1. Magnitude of estimated rates and strength of support for specific rate shifts in the passerine tree. Shown are the marginal odds ratios (the ratio of the posterior to the prior probabilities of a rate shift on each corresponding branch) for the 14 branches with the highest ratios, along with the median estimated speciation and extinction rates for passerines as a whole, and for each rate-shifted clade. For each clade, evidence for a diversification rate shift at a corresponding clade in the analyses of Jetz *et al*. (113) is also shown (strong=shift found for ≥ 50% of synthetic trees, weak=shift found in < 50% of synthetic trees, none=no shift found).

Clade	Marginal Odds Ratio	Median Speciation Rate	Median Extinction Rate	Fold Increase Over Background	Evidence in Jetz *et al.* (113)
Passerine background	—	0.109	0.006	1.00	—
Muscicapoidea excluding Cinclidae and Elachuridae	24328.2	0.297	0.031	2.58	Weak
Clade comprising Cisticolidae, Locustelloidea, Pnoepygidae, Hirundinidae, Sylvioidea, and Aegithaloidea	22465.5	0.271	0.037	2.27	Weak
Passerida excluding Promeropidae	16591.6	0.324	0.045	2.71	Strong[1]
Thraupidae	11717.7	0.494	0.057	4.24	None
Parulidae excluding genus *Seiurus*	10383.1	0.764	0.127	6.18	None
Thamnophilidae assigned to *Thamnophilus* (subfamily Thamnophilinae)	10347.7	0.382	0.031	3.41	None
Corvidae excluding genus *Pyrrhocorax*	9034.8	0.481	0.084	3.85	None
Tyrannidae excluding subfamily Hirundineinae	8020.4	0.422	0.048	3.63	None
Clade comprising Rhynchocyclidae and Tyrannidae	6125.6	0.358	0.053	2.96	None
Clade comprising Dendrocolaptidae and Furnariidae	5632.5	0.337	0.050	2.79	Strong
Icteridae excluding genera *Icteria, Xanthocephalus, Dolichonyx,* and *Sturnella*	5598.8	0.566	0.089	4.63	None
Corvides excluding Cinclosomatidae	5242.3	0.234	0.044	1.84	Weak
Rhynchocyclidae	3582.0	0.277	0.042	2.28	None
Monarchidae	2710.6	0.401	0.085	3.07	None

[1]This clade corresponds to clade X of Jetz *et al*. (113), with the addition of sunbirds (Nectariniidae), flowerpeckers (Dicaeidae), leafbirds (Chloropseidae) and fairy bluebirds (Irenidae). Although not identical, it is likely that the two analyses reflect the same underlying rate shift.

Table S2. Summary of results from BAMM analysis of the passerine portion of 100 trees from the Stage 2 (Hackett *et al*. 114 backbone) posterior distribution generated by Jetz *et al*. (113). Shown are the top 15 clades most frequently found to have the highest marginal odds ratio of a rate shift.

Clade	Description	Monophyletic in UCE tree	Shift in UCE tree	Shift similar to shift in UCE tree	% of Jetz trees with shift	Evidence in Jetz *et al*. (113)[1]
1	Furnariidae and Dendrocolaptidae	Yes	Yes	Yes (identical)	88	Strong (N)
2	Most Emberizoids (minus Calcariidae)	No	NA	No (three separate shifts within this clade)	62	None
3	Thamnophilidae	Yes	Yes	Yes (identical)	53	None
4	OW Warblers and allies	No	NA	No	52	Weak (S)
5	Darwin's finches and allies	Not sampled	NA	Not sampled	50	None
6	Sylvioids	No	NA	Yes (similar)	47	Weak (R)
7	Darwin's finches and allies	Not sampled	NA	Not sampled	45	None
8	*Sporophila* tanagers	Not sampled	NA	Not sampled	36	None
9	Muscicapoids and Certhioids	No	NA	Yes (Muscicapoids only)	32	Weak (V)
10	Darwin's finches and allies	Not sampled	NA	Not sampled	31	None
11	Most core corvoids	No	NA	Yes (similar)	28	Weak (P)
12	Emberizoids plus Motacillidae and Fringillidae	Yes	No	No	23	None
13	Babblers and white eyes	No	NA	No	17	Strong (T)
14	Tyrannidae minus Hirundineinae	Yes	Yes	Yes (identical)	16	None
15	Carduelinae	Not sampled	NA	Not sampled	16	None

[1]Letters corresponding to node designations in Jetz *et al*. (113) are given.

Table S3. Comparison of biogeographic models in BioGeoBEARS. LnL = natural logarithm of likelihood; *d* = dispersal rate; *e* = extinction rate; *j* = jump-dispersal rate; AIC = Akaike Information Criterion.

Model	LnL	No. of Parameters	*d*	*e*	*j*	AIC
Unrestricted dispersal DEC	-564.55	2	0.0086	0.00		1133
Restricted dispersal DEC	-456.32	2	0.0253	0.00		917
Unrestricted dispersal DEC + *j*	-548.98	3	0.0079	0.00	0.0202	1104
Restricted dispersal DEC + *j*	-438.93	3	0.0230	0.00	0.0710	884

Additional Supplementary Files

Supplementary File S1 (S1.xlsx). Sampling and sequence data characteristics.

Supplementary File S2 (S2.nexus.txt). Phylogenetic tree files in nexus format from concatenation and coalescent analyses of the entire dataset and subsets of the data matrix.

Supplementary File S3 (S3.xlsx). Subsampling and trimming strategy for phylogenetic analysis.

References

1. Glenn TC, et al. (2016) Adapterama I: Universal stubs and primers for thousands of dual-indexed Illumina libraries (iTru & iNext). *bioRxiv*:https://doi.org/10.1101/049114.
2. Rohland N, Reich D (2011) Cost-effective , high-throughput DNA sequencing. *Genome Res*:939–946.
3. Faircloth BC, et al. (2012) Ultraconserved elements anchor thousands of genetic markers spanning multiple evolutionary timescales. *Syst Biol* 61:717–26.
4. Faircloth BC (2015) PHYLUCE is a software package for the analysis of conserved genomic loci. *Bioinformatics* 32:786–788.
5. Grabherr MG, et al. (2011) Full-length transcriptome assembly from RNA-Seq data without a reference genome. *Nat Biotechnol* 29:644–652.
6. Nurk S, et al. (2013) Assembling genomes and mini-metagenomes from highly chimeric reads. *Research in Computational Molecular Biology. RECOMB 2013. Lecture Notes in Computer Science. Vol 7821*, eds Deng M, Jiang R, Sun F, Zhang X (Springer, Berlin, Heidelberg), pp 158–170.
7. Faircloth BC (2018) Tutorial I: UCE Phylogenomics. Available at: http://phyluce.readthedocs.io/en/latest/tutorial-one.html [Accessed August 6, 2018].
8. Katoh K, Standley DM (2013) MAFFT multiple sequence alignment software version 7: improvements in performance and usability. *Mol Biol Evol* 30:772–80.
9. Castresana J (2000) Selection of conserved blocks from multiple alignments for their use in phylogenetic analysis. *Mol Biol Evol* 17:540–552.
10. Kozlov AM, Aberer AJ, Stamatakis A (2015) ExaML version 3: A tool for phylogenomic analyses on supercomputers. *Bioinformatics* 31:2577–2579.
11. Stamatakis A (2014) RAxML version 8: a tool for phylogenetic analysis and post-analysis of large phylogenies. *Bioinformatics* 30:1312–1313.
12. Chifman J, Kubatko L (2015) Identifiability of the unrooted species tree topology under the coalescent model with time-reversible substitution processes, site-specific rate variation, and invariable sites. *J Theor Biol* 374:35–47.
13. Chifman J, Kubatko L (2014) Quartet inference from SNP data under the coalescent model. *Bioinformatics* 30:3317–3324.
14. Vachaspati P, Warnow T (2015) ASTRID: Accurate Species TRees from Internode Distances. *BMC Genomics* 16:S3.
15. Liu L, Yu L (2011) Estimating species trees from unrooted gene trees. *Syst Biol* 60:661–667.
16. Mirarab S, Warnow T (2015) ASTRAL-II: Coalescent-based species tree estimation with many hundreds of taxa and thousands of genes. *Bioinformatics* 31:i44–i52.
17. Liu L, Yu L, Pearl DK, Edwards S V (2009) Estimating species phylogenies using coalescence times among sequences. *Syst Biol* 58:468–77.
18. Seo TK (2008) Calculating bootstrap probabilities of phylogeny using multilocus sequence data. *Mol Biol Evol* 25:960–971.
19. Swofford DL (2003) *PAUP*. Phylogenetic analysis using parsimony (*and Other Methods)* (Sinauer Associates, Sunderland, Massachusetts).
20. Snir S, Rao S (2012) Quartet MaxCut: A fast algorithm for amalgamating quartet trees. *Mol Phylogenet Evol* 62:1–8.
21. Kubatko LS, Degnan JH (2007) Inconsistency of phylogenetic estimates from concatenated data under coalescence. *Syst Biol* 56:17–24.
22. Huang H, He Q, Kubatko LS, Knowles LL (2010) Sources of error inherent in species-tree estimation: Impact of mutational and coalescent effects on accuracy and implications for choosing among different methods. *Syst Biol* 59:573–583.
23. Oliveros CH (2015) Phylogenomics of rapid avian radiations. Dissertation (University of Kansas). Available at: https://kuscholarworks.ku.edu/handle/1808/21553.
24. Hosner PA, Faircloth BC, Glenn TC, Braun EL, Kimball RT (2016) Avoiding missing data biases in phylogenomic inference: an empirical study in the landfowl (Aves: Galliformes). *Mol Biol Evol*

33:1110–1125.
25. Moyle RG, et al. (2016) Tectonic collision and uplift of Wallacea triggered the global songbird radiation. *Nat Commun* 7:12709.
26. Sayyari E, Whitfield JB, Mirarab S (2017) Fragmentary gene sequences negatively impact gene tree and species tree reconstruction. *Mol Biol Evol* 34:3279–3291.
27. Mayr G (2016) *Avian evolution: the fossil record of birds and its paleobiological significance* (John Wiley & Sons, Chichester, West Sussex).
28. Heath TA, Huelsenbeck JP, Stadler T (2014) The fossilized birth–death process for coherent calibration of divergence-time estimates. *Proc Natl Acad Sci U S A* 111:E2957–E2966.
29. Parham JF, et al. (2012) Best practices for justifying fossil calibrations. *Syst Biol* 61:346–359.
30. Claramunt S, Cracraft J (2015) A new time tree reveals Earth history's imprint on the evolution of modern birds. *Sci Adv* 1:e1501005.
31. Ho SYW, Phillips MJ (2009) Accounting for calibration uncertainty in phylogenetic estimation of evolutionary divergence times. *Syst Biol* 58:367–380.
32. Prum RO, et al. (2015) A comprehensive phylogeny of birds (Aves) using targeted next-generation DNA sequencing. *Nature* 526:569–573.
33. Selvatti AP, Gonzaga LP, Russo CADM (2015) A Paleogene origin for crown passerines and the diversification of the oscines in the New World. *Mol Phylogenet Evol* 88:1–15.
34. Drummond AJ, Suchard MA, Xie D, Rambaut A (2012) Bayesian phylogenetics with BEAUti and the BEAST 1.7. *Mol Biol Evol* 29:1969–1973.
35. Rambaut A, Drummond AJ (2014) Tracer v.1.6. Available at: http://tree.bio.ed.ac.uk/software/tracer/.
36. Rambaut A, Drummond AJ (2016) TreeAnnotator V. 1.8.4. Available at: http://tree.bio.ed.ac.uk/software/beast/.
37. Rambaut A, Drummond AJ (2016) LogCombiner v. 1.8.4. Available at: http://tree.bio.ed.ac.uk/software/beast/.
38. Brown JW, Smith SA (2018) The past sure is tense: on interpreting phylogenetic divergence time estimates. *Syst Biol* 67:340–353.
39. Smith SA, Brown JW, Walker JF (2018) So many genes, so little time: A practical approach to divergence-time estimation in the genomic era. *PLoS One* 13:e0197433.
40. dos Reis M, Yang Z (2011) Approximate likelihood calculation on a phylogeny for Bayesian estimation of divergence times. *Mol Biol Evol* 28:2161–2172.
41. Rabosky DL (2015) No substitute for real data: A cautionary note on the use of phylogenies from birth-death polytomy resolvers for downstream comparative analyses. *Evolution* 69:3207–3216.
42. Matzke NJ (2013) BioGeoBEARS: BioGeography with Bayesian (and Likelihood) Evolutionary Analysis in R Scripts. Ph.D. Thesis. University of California, Berkeley.
43. R Development Core Team (2008) R: A language and environment for statistical computing. R Foundation for Statistical Computing. Vienna, Austria. ISBN 3-900051-07-0. URL http://www.r-project.org.
44. Clark JR, et al. (2008) A comparative study in ancestral range reconstruction methods: retracing the uncertain histories of insular lineages. *Syst Biol* 57:693–707.
45. Ree RH, Smith SA (2008) Maximum likelihood inference of geographic range evolution by dispersal, local extinction, and cladogenesis. *Syst Biol* 57:4–14.
46. Matzke NJ (2014) Model selection in historical biogeography reveals that founder-event speciation is a crucial process in island clades. *Syst Biol* 63:951–970.
47. Ree RH, Sanmartín I (2018) Conceptual and statistical problems with the DEC+J model of founder-event speciation and its comparison with DEC via model selection. *J Biogeogr* 45:741–749.
48. Hansen J, Sato M, Russell G, Kharecha P (2013) Climate sensitivity, sea level and atmospheric carbon dioxide. *Philos Trans R Soc A* 371:20120294.
49. Stadler T (2011) Mammalian phylogeny reveals recent diversification rate shifts. *Proc Natl Acad Sci U S A* 108:6187–6192.
50. Höhna S (2015) The time-dependent reconstructed evolutionary process with a key-role for mass-

extinction events. *J Theor Biol* 380:321–331.
51. Höhna S, et al. (2016) RevBayes: Bayesian phylogenetic inference using graphical models and an interactive model-specification language. *Syst Biol* 65:726–736.
52. Höhna S, et al. (2017) Statistical phylogenetic inference using RevBayes. Available at: https://github.com/revbayes/revbayes_tutorial/raw/master/tutorial_TeX/RB_Manual.pdf.
53. Dickinson E, Christidis L (2014) *The Howard & Moore complete checklist of the birds of the world. 4th Edition, Vol. 2* eds Dickinson E, Christidis L (Aves Press, Eastbourne, U.K.). 4th Ed.
54. Rabosky DL (2014) Automatic detection of key innovations, rate shifts, and diversity-dependence on phylogenetic trees. *PLoS One* 9:e89543.
55. Dyke GJ, Cooper JH (2000) A new psittaciform bird from the London Clay (Lower Eocene) of England. *Palaeontology* 43:271–285.
56. Mayr G (2002) On the osteology and phylogenetic affinities of the Pseudasturidae–Lower Eocene stem-group representatives of parrots (Aves, Psittaciformes). *Zool J Linn Soc* 136:715–729.
57. Ksepka DT, Balanoff AM, Bell MA, Houseman MD (2013) Fossil grebes from the Truckee Formation (Miocene) of Nevada and a new phylogenetic analysis of Podicipediformes (Aves). *Palaeontology* 56:1149–1169.
58. Mayr G (2015) A reassessment of Eocene parrotlike fossils indicates a previously undetected radiation of zygodactyl stem group representatives of passerines (Passeriformes). *Zool Scr* 44:587–602.
59. Westerhold T, et al. (2007) On the duration of magnetochrons C24r and C25n and the timing of early Eocene global warming events: Implications from the Ocean Drilling Program Leg 208 Walvis Ridge depth transect. *Paleoceanography* 22. doi:10.1029/2006PA001322.
60. Woodburne MO, et al. (2014) Revised timing of the South American early Paleogene land mammal ages. *J South Am Earth Sci* 54:109–119.
61. Weidig I (2010) New birds from the Lower Eocene Green River Formation, North America. In Proceedings of the VII International Meeting of the Society of Avian Paleontology and Evolution, ed. W.E. Boles and T.H. Worthy. *Rec Aust Museum* 62:29–44.
62. Mayr G (2008) Phylogenetic affinities of the enigmatic avian taxon *Zygodactylus* based on new material from the early oligocene of France. *J Syst Palaeontol* 6:333–344.
63. Boles WE (1995) The world's oldest songbird. *Nature* 374:21–22.
64. Smith ME, Chamberlain KR, Singer BS, Carroll AR (2010) Eocene clocks agree: Coeval 40Ar/39Ar, U-Pb, and astronomical ages from the Green River Formation. *Geology* 38:527–530.
65. Harrison C, Walker C (1977) Birds of the British Lower Eocene. *Tert Res Spec Pap* 3:1–52.
66. Wetmore A (1936) Two new species of hawks from the Miocene of Nebraska. *Proc United States Natl Museum* 84:73–78.
67. Li Z, Zhou Z, Deng T, Li Q, Clarke JA (2014) A falconid from the Late Miocene of northwestern China yields further evidence of transition in Late Neogene steppe communities. *Auk* 131:335–350.
68. Becker J (1987) Revision of *"Falco" ramenta* Wetmore and the Neogene evolution of the Falconidae. *Auk*:270–276.
69. Mayr G (2009) *Paleogene Fossil Birds* (Springer Berlin Heidelberg, Berlin, Heidelberg) doi:10.1007/978-3-540-89628-9.
70. Worthy TH, Tennyson AJD, Scofield RP (2011) An early Miocene diversity of parrots (Aves, Strigopidae, Nestorinae) from New Zealand. *J Vertebr Paleontol* 31:1102–1116.
71. Pole M, Douglas B (1998) A quantitative palynostratigraphy of the Miocene Manuherikia Group, New Zealand. *J R Soc New Zeal* 28:405–420.
72. Landis CA, et al. (2008) The Waipounamu Erosion Surface: questioning the antiquity of the New Zealand land surface and terrestrial fauna and flora. *Geol Mag* 145:173–197.
73. Trewick SA, Gibb GC (2010) Vicars, tramps and assembly of the New Zealand avifauna: a review of molecular phylogenetic evidence. *Ibis (Lond 1859)* 152:226–253.
74. Worthy TH, et al. (2010) Biogeographical and phylogenetic implications of an early Miocene wren (Aves: Passeriformes: Acanthisittidae) from New Zealand. *J Vertebr Paleontol* 30:479–498.
75. Mitchell KJ, et al. (2016) Ancient mitochondrial genomes clarify the evolutionary history of New

Zealand's enigmatic acanthisittid wrens. *Mol Phylogenet Evol* 102:295–304.
76. Mayr G, Manegold A (2006) New specimens of the earliest European passeriform bird. *Acta Palaeontol Pol* 51:315–323.
77. Gradstein F, Ogg J, Schmitz M, Ogg G (2012) *Geological Time Scale 2012* (Elsevier Science and Technology, Amsterdam).
78. Mayr G, Manegold A (2004) The oldest European fossil songbird from the early Oligocene of Germany. *Naturwissenschaften* 91:173–177.
79. Ballman P (1969) Die Vögel aus der altburdigalen Spaltenfüllung von Wintershof (West) bei Eichstätt in Bayern. *Zitteliana*:5–61.
80. Manegold A, Mayr G, Mourer-Chauviré C (2004) Miocene songbirds and the composition of the European passeriform avifauna. *Auk* 121:1155–1160.
81. Boles WE (1995) A preliminary analysis of the Passeriformes from Riversleigh, northwestern Queensland, Australia, with the description of a new species of lyrebird. *Cour Forschungsinstitut Senckenb* 181:163–170.
82. Dunning J (2007) *CRC Handbook of Avian Body Masses, Second Edition* (CRC Press).
83. Rich P, McEvey A, Baird R (1985) Osteological comparison of the scrub-birds, *Atrichornis*, and lyrebirds, *Menura* (Passeriformes: Atrichornithidae and Menuridae). *Rec Aust Museum* 37:165–191.
84. Woodhead J, et al. (2016) Developing a radiometrically-dated chronologic sequence for Neogene biotic change in Australia, from the Riversleigh World Heritage Area of Queensland. *Gondwana Res* 29:153–167.
85. Arena DA, et al. (2016) Mammalian lineages and the biostratigraphy and biochronology of Cenozoic faunas from the Riversleigh World Heritage Area, Australia. *Lethaia* 49:43–60.
86. Boles WE (2005) Fossil honeyeaters (Meliphagidae) from the Late Tertiary of Riversleigh, north-western Queensland. *Emu - Austral Ornithol* 105:21–26.
87. Creaser P (1997) Oligocene-Miocene sediments of Riversleigh: the potential significance of topography. *Mem Museum* 41:303–314.
88. Travouillon KJ, Archer M, Hand SJ, Godthelp H (2006) Multivariate analyses of Cenozoic mammalian faunas from Riversleigh, northwestern Queensland. *Alcheringa An Australas J Palaeontol* 30:323–349.
89. Archer M, et al. (2006) Current status of species-level representation in faunas from selected fossil localities in the Riversleigh World Heritage Area, northwestern Queensland. *Alcheringa An Australas J Palaeontol* 30:1–17.
90. Archer M, Hand S, Godthelp H, Creaser P (1997) Correlation of the Cainozoic sediments of the Riversleigh World Heritage fossil property, Queensland, Australia. *Mémoires Trav l'Institut Montpellier* 21:131–152.
91. Boles WE (1993) A logrunner *Orthonyx* (Passeriformes: Orthonychidae) from the Miocene of Riversleigh, northwestern Queensland. *Emu* 93:44–49.
92. Nguyen JMT, Boles WE, Worthy TH, Hand SJ, Archer M (2014) New specimens of the logrunner *Orthonyx kaldowinyeri* (Passeriformes: Orthonychidae) from the Oligo-Miocene of Australia. *Alcheringa* 38(2):245–255.
93. Travouillon KJ, Legendre S, Archer M, Hand SJ (2009) Palaeoecological analyses of Riversleigh's Oligo-Miocene sites: implications for Oligo-Miocene climate change in Australia. *Palaeogeogr Palaeoclimatol Palaeoecol* 276:24–37.
94. Archer M, Godthelp H, Hand S, Megirian D (1989) Fossil mammals of Riversleigh, Northwestern Queensland: preliminary overview of biostratigraphy, correlation and environmental change. *Aust Zool* 25:29–66.
95. Nguyen J (2016) Australo-Papuan treecreepers (Passeriformes: Climacteridae) and a new species of sittella (Neosittidae: *Daphoenositta*) from the Miocene of Australia. *Palaeontol Electron*. doi:10.26879/602.
96. Travouillon KJ, Escarguel G, Legendre S, Archer M, Hand SJ (2011) The use of MSR (Minimum Sample Richness) for sample assemblage comparisons. *Paleobiology* 37:696–709.
97. Worthy TH, Tennyson AJD, Jones C, McNamara JA, Douglas BJ (2007) Miocene waterfowl and

other birds from central Otago, New Zealand. *J Syst Palaeontol* 5:1–39.
98. Nguyen JMT, Worthy TH, Boles WE, Hand SJ, Archer M (2013) A new cracticid (Passeriformes : Cracticidae) from the Early Miocene of Australia. *Emu* 113:374.
99. Steadman DW (1981) A re-examination of *Palaeostruthus hatcheri* (Shufeldt), a late Miocene sparrow from Kansas. *J Vertebr Paleontol* 1:171–173.
100. Janis C, Gunnell G, Uhen M (2008) *Evolution of Tertiary Mammals of North America. Volume 2: Small Mammals, Xenarthrans, and Marine Mammals* (Cambridge University Press, Cambridge).
101. Howard H (1957) A new species of passerine bird from the Miocene of California. *Los Angeles Cty Museum Nat Hist Contrib Sci* 9:1–16.
102. Brodkorb P (1972) Neogene fossil jays from the Great Plains. *Condor* 74:347–349.
103. Manegold A (2008) Earliest fossil record of the Certhioidea (treecreepers and allies) from the early Miocene of Germany. *J Ornithol* 149:223–228.
104. Mein P (1999) European Miocene mammal biochronology. *Miocene L Mamm Eur*:25–38.
105. Steininger F (1999) Chronostratigraphy, geochronology and biochronology of the Miocene "European Land Mammal Mega-Zones" (ELMMZ) and the Miocene "Mammal-Zones (MN-Zones)." *Miocene L Mamm Eur*:9–24.
106. del Hoyo J, Collar N (2016) *HBW and BirdLife International Illustrated Checklist of the Birds of the World. Volume 2: Passerines* (Lynx Edicions, Barcelona).
107. Sefc KM, Payne RB, Sorenson MD (2003) Phylogenetic relationships of African sunbird-like warblers: Moho (*Hypergerus atriceps*), Green Hylia (*Hylia prasina*) and Tit-hylia (*Pholidornis rushiae*). *Ostrich* 74:8–17.
108. Fregin S, Haase M, Olsson U, Alström P (2012) New insights into family relationships within the avian superfamily Sylvioidea (Passeriformes) based on seven molecular markers. *BMC Evol Biol* 12:157.
109. Bates GL (1930) *Handbook of the birds of West Africa* (Bale, Sons and Danielson, London).
110. Alström P, et al. (2014) Discovery of a relict lineage and monotypic family of passerine birds. *Biol Lett* 10:5.
111. Gill FB, Donsker D (2018) *IOC World Bird List (v. 8.1)* eds Gill FB, Donsker D (http://www.worldbirdnames.org/) doi:10.14344/IOC.ML.8.1.
112. Hall R (2009) Southeast Asia's changing palaeogeography. *Blumea J Plant Taxon Plant Geogr* 54:148–161.
113. Jetz W, Thomas GH, Joy JB, Hartmann K, Mooers AO (2012) The global diversity of birds in space and time. *Nature* 491:444–448.
114. Hackett SJ, et al. (2008) A phylogenomic study of birds reveals their evolutionary history. *Science* 320:1763–1768.
115. Burns KJ, et al. (2014) Phylogenetics and diversification of tanagers (Passeriformes: Thraupidae), the largest radiation of Neotropical songbirds. *Mol Phylogenet Evol* 75:41–77.